# DESIGN AND ANALYSIS OF HIGH PERFORMANCE PHOTONIC CRYSTAL NANOCAVITY

A dissertation submitted in partial fulfillment
of the requirement for the award of degree of

**MASTER OF ENGINEERING**

**IN**

**ELECTRONICS & COMMUNICATION ENGINEERING**


Submitted by:

**Sakshi Aneja**

**(801261018)**

Under the supervision of

**Dr. Mukesh Kumar**



**DEPARTMENT OF ELECTRONICS & COMMUNICATION ENGINEERING**

**THAPAR UNIVERSITY**
(Established under the section 3 of UGC Act, 1956)
PATIALA-147004 (PUNJAB)
INDIA



JULY – 2014

# DECLARATION

I hereby declare that the work presented in this dissertation entitled **"Design and Analysis of High performance Photonic Crystal Nanocavity"**, is an authentic record of my study carried out for the requirement of the award of degree of M.E. (Electronics and Communication Engineering) at Thapar University, Patiala, under the supervision of Dr. Mukesh Kumar.

The matter presented in this dissertation has not been submitted in any other university/institute for the award of any other degree. Except where references have been given in text, it is entirely the authors own work.

Sakshi

Date: 11-07-2014

**Sakshi Aneja**
Roll No.: 801261018

It is certified that the above statement made by the student is correct to the best of my knowledge and belief.

11/7/2014

Date: 11-07-2014

**Dr. Mukesh Kumar**
Assistant Professor, ECED
Thapar University, Patiala

Countersigned by:

**Dr. Sanjay Sharma**
Professor and Head, ECED
Thapar University, Patiala

**Dr. S.K. Mohapatra**
Dean of Academic Affairs
Thapar University, Patiala

# CONTENTS

**Acknowledgement** **i**

**Abstract** **ii**

**List of Figures** **iii**

**List of Tables** **v**

**Glossary of Acronyms** **vi**

**CHAPTER 1: INTRODUCTION ..... 1**

1.1 Integrated Optoelectronics ..... 1

1.2 Photonic Crystals ..... 3

1.2.1 Maxwell Equations in Photonic Crystals ..... 4

1.2.2 Types of Photonic Crystals ..... 6

1.3 Photonic Crystal Slabs ..... 7

1.4 Applications of Photonic Crystals ..... 9

1.5 Thesis Objective ..... 10

1.6 Format of Thesis ..... 10

**CHAPTER 2: PHOTONIC CRYSTAL CAVITIES ..... 12**

2.1 General ..... 12

2.2 Types of Photonic Crystal Cavities ..... 13

2.2.1 Hexagonal Cavities ..... 13

2.2.2 Linear Cavities ..... 15

2.2.3 Double Heterostructure Cavities ..... 17

2.3 Quality Factor and Mode Volume ..... 18

2.3.1 Q-factor ..... 18

2.3.2 Mode Volume ..... 20

2.4 Importance of Photonic Crystal Nanocavities ..... 21

**CHAPTER 3: LITERATURE SURVEY ..... 22**

**CHAPTER 4: DESIGN AND ANALYSIS OF HIGH-Q PHOTONIC CRYSTAL NANOCAVITY .....38**

4.1 Structure of Photonic Crystal Nanocavity .....38

4.2 Meep for Computational Modelling of Cavity Design.....41

4.3 Methodology for the design of Photonic Crystal Nanocavity.....41

4.4 Enhancement of Q-factor.....43

4.4.1 Analysis of Electric Field Distribution.....43

4.4.2 Electric Field profile and Energy density .....45

4.4.3 Design Approach.....46

4.4.4 Calculation of Resonant Wavelength and Spectral Width .....53

4.4.5 Calculation of Photon lifetime .....53

4.4.6 Effect of increasing slab thickness .....54

4.5 Comparison with L3 cavity having six air-hole shifts.....54

**CHAPTER 5: CONCLUSION & FUTURE SCOPE.....57**

**REFERENCES .....58**

# ACKNOWLEDGEMENT

A dissertation cannot be completed without the help of many people who contribute directly or indirectly through their constructive criticism in the evolution and preparation of this work. It would not be fair on my part, if I don't say a word of thanks to all those whose sincere advice made this period a real educative, enlightening, pleasurable and memorable one.

First of all, a special debt of gratitude is owned to my supervisor, Dr. Mukesh Kumar for his gracious efforts and keen pursuits, which has remained as a valuable asset for the successful completion of research work. His dynamism and diligent enthusiasm has been highly instrumental in keeping my spirit high. The flawless and forthright suggestions blended with an innate intelligent application have crowned my task a success.

I also like to offer my sincere thanks to all faculty members, teaching and non-teaching staff of Electronics and Communication Engineering Department (ECED), and staff of central library, TU, Patiala for their assistance.

I am extremely thankful to my parents, brother, sister and friends for their constant encouragement during the entire course of my research work.

# ABSTRACT

Photonic Crystal Nanocavities are getting significant attention because of their potential of trapping and storing photons in a small region of nanometer range and enhancing light interaction with various functional materials and structures. A strong light-matter interaction is obtained in high quality photonic crystal nanocavities that strongly confine photons in a small cavity region of optical wavelength dimension. Because of their capability to confine and manipulate photons in nanometer scales, high-Q PhC nanocavities find applications in various fields, such as photonics, telecommunications, quantum information and cavity quantum electrodynamics.

The present work aims at designing, simulation and analysis of a L3 photonic crystal nanocavity. This work is directed towards designing a cavity structure which has a single mode with ultra-high Q-factor and small mode volume, confined in the cavity. A high Q-factor and small mode volume gives a large Q/V and enhances the Purcell factor. The optimization is done in order to get better temporal and spatial confinement of the confined resonant mode in the nanocavity. The research work is performed on a thin photonic crystal slab made out of gallium arsenide with a triangular array of air holes. L3 type defect is created in the crystal with three missing air-holes in the center of the slab. The cavity structure is designed by shifting four nearest neighbour air-holes on cavity edges and shrinking first nearest neighbour air-holes. By fine-tuning the four nearest neighbour air-holes on cavity edges, the electric field profile can be tailored. As a result, we have obtained a single cavity mode at resonant frequency 0.258 c/a with Q-factor 493681, mode volume $0.828(\lambda/n)^3$ and $Q/V_{mode}$ of $615152(\lambda/n)^{-3}$. This design improves the quality factor by a factor of 84 and $Q/V_{mode}$ by a factor of 70 in comparison to unoptimised L3 photonic crystal nanocavity.

Such photonic crystal nanocavities lead to very large Purcell factor because of their ultra-high Q-factor and ultra-small cavity mode volume. They can be used for realization of quantum computing platform by coupling with quantum dots and nanocavity lasers.

# LIST OF FIGURES


**1.1** Electronic Integrated Circuit, Bundle of Optical Fibres and Photonic Circuit ..... 2

**1.2** Analogy of atomic lattice in a semiconductor and photonic crystal lattice..... 3

**1.3** One-,Two-, and Three- dimensional photonic crystals..... 6

**1.4** Photonic crystal slab structure patterned with a triangular lattice..... 7

**1.5** Explanation of the light line concept for light guiding in the slab..... 8

**2.1** Photonic Crystal Hexagonal Cavity ..... 13

**2.2** Photonic Crystal L3 Cavity..... 15

**2.3** Photonic Crystal L5 Cavity..... 16

**2.4** Photonic Crystal L7 Cavity..... 16

**2.5** Photonic Crystal Double Heterostructure Cavity ..... 17

**4.1** 3D View of Dielectric profile of proposed high-Q L3 Nanocavity Design..... 39

**4.2** 2D View of Dielectric profile of proposed high-Q L3Nanocavity Design..... 40

**4.3** Electric field distribution of confined cavity mode ..... 44

**4.4** Fourier transformed Electric Field of confined cavity mode..... 44

**4.5** Electric Field (Ey) profile of single mode confined in L3 Cavity.... 45

**4.6** Electric field energy density of confined cavity mode ..... 46

**4.7** Variation of Q-factor, $V_{mode}$ and $Q/V_{mode}$ with 'A' air-hole displacements..... 48

**4.8** Variation of Q-factor, $V_{mode}$ and $Q/V_{mode}$ with 'B' air-hole displacements..... 49

**4.9** Variation of Q-factor, $V_{mode}$ and $Q/V_{mode}$ with 'C' air-hole displacements..... 50

**4.10** Variation of Q-factor, $V_{mode}$ and $Q/V_{mode}$ with 'A' air-hole radii ..... 51
**4.11** Variation of Q-factor, $V_{mode}$ and $Q/V_{mode}$ with 'D' air-hole displacements ..... 52
**4.12** Comparison of spatial fourier transformed electric field for two optimised cavity structures ..... 55

# LIST OF TABLES

**4.1** Step-by-step approach for L3 Cavity Design ..... 46
**4.2** Effect of increasing slab thickness ..... 54

# GLOSSARY OF ACRONYMS

| | |
|---|---|
| **1D** | One-dimensional |
| **2D** | Two-dimensional |
| **3D** | Three-dimensional |
| **DBR** | Distributed Bragg Reflection |
| **EPIC** | Electronic and Photonic Integrated Circuit |
| **FDTD** | Finite Difference Time Domain |
| **LASER** | Light Amplification by Stimulated Emission of Radiation |
| **MATlab** | Matrix Laboratory |
| **MEEP** | MIT Electromagnetic Equation Propagation |
| **MPB** | MIT Photonics Bands |
| **NB** | Nanobeam |
| **PBG** | Photonic Band Gap |
| **PCS** | Photonic Crystal Slab |
| **PhC** | Photonic Crystal |
| **Q** | Quality factor |
| **SOI** | Silicon on Insulator |
| **TE** | Transverse Electric |
| **TM** | Transverse Magnetic |
| **TIR** | Total Internal Reflection |
| **VCSEL** | Vertical Cavity Surface Emitting Lasers |

# CHAPTER 1
# INTRODUCTION

## 1.1 Integrated Optoelectronics

The semiconductor technology has played a major role in almost every aspect of our day-to-day life and changed the world beyond anything. However, the drive towards miniaturization and high-speed performance of integrated electronic circuits has induced considerable research effort in every corner of the world. Unfortunately, miniaturization of circuit results in increased resistance and greater levels of power dissipation. Also, the demand for higher speed in circuits leads to a highly sensitive signal synchronization. In an attempt to further the advancement of high-density integration and system performance, scientists have turned towards light instead of electrons as the information carrier. Light has numerous advantages over the electron. It can travel in a dielectric material at much higher speed than an electron in a metallic wire. Light can also carry tremendous amount of information per second. Moreover, the bandwidth is significantly larger in case of dielectric materials in comparison to metals. The bandwidth in fibre-optic communication systems is of the order of one terahertz, while it is only a few hundred kilohertz in electronic systems (such as the telephone) [1,2]. Furthermore, energy losses are also reduced when light is used as a carrier because photons do not interact as strongly as electrons. **Fig. 1.1(a)** and **(b)** shows an electronic integrated circuit and a bundle of optical fibres respectively. Despite so many advantages of photons, all-optical circuits are not yet available commercially on a large scale. Although, the performance of electronic circuits has been improved significantly with the advent of some hybrid optoelectronic circuits, but the main challenge lies in the design of a multipurpose optical component in comparison to an electronic transistor and this has severely obstructed the advancement of all-optical systems. From the last 27 years, a new class of optical materials known as photonic crystals [1] has gathered significant attention and is anticipated to hold the key towards all-optical integrated circuits. The concept of this new class of optical materials has been given by Yablonovitch [3] and John [4]. The fundamental behind the design of photonic crystals is to design a material such that it affects the properties of

photons just like an ordinary semiconductor crystal affect the properties of electrons.

(a)

(b)

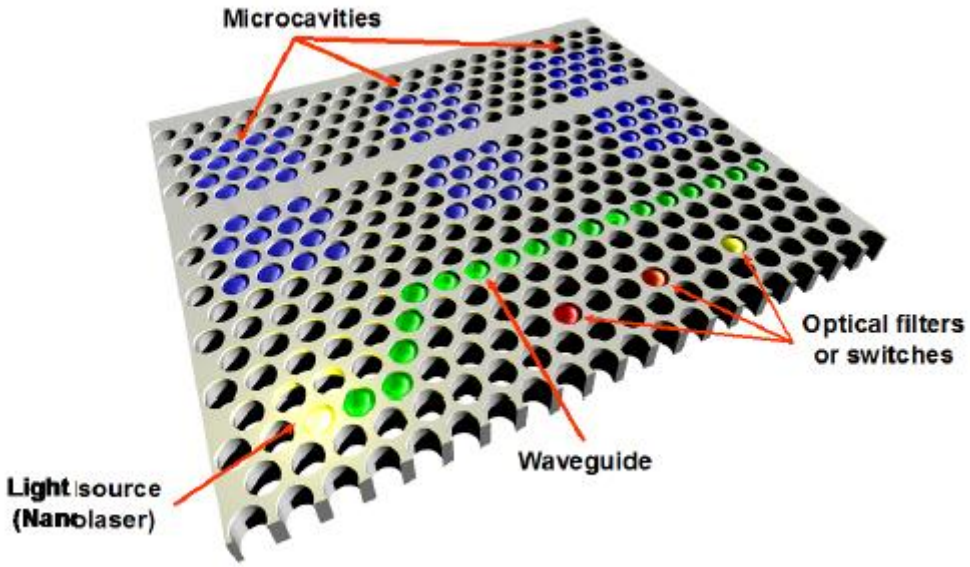


(c)

**Fig. 1.1:** (a) Electronic Integrated Circuit (b) Bundle of Optical Fibres (c) Photonic Circuit [2]

Both Yablonovitch and John suggested that the nature of photonic modes in a material can be influenced by designing a structure that has periodically varying dielectric constant. Yablonovitch's research was aimed at controlling the radiative properties of materials, while John's research was to affect the photon localization by introducing a random refractive-index variation. **Fig. 1.1(c)** shows a photonic

circuit. Traditionally, total internal reflection (TIR) is used as a mechanism for the manipulation of optical photons, e.g., in optical fibres. Due to TIR, the light propagates in a high-dielectric material and is reflected at the interface with a low-dielectric material. But, this requires a smooth interface with respect to the wavelength of light and therefore, the degree of miniaturization of optical components is severely limited. Photonic crystals provide a totally different mechanism for the control of light. The underlying concept of photonic crystals is Distributed Bragg Reflection by the periodically varying crystal resulting in photonic band gap, which is the optical analogue of electronic band gap in semiconductors [5]. The electronic and photonic integrated circuits (EPIC) i.e., the circuits that integrate photonic devices with microelectronic circuits, has the potential to realize low cost and high performance optical systems.

## 1.2 Photonic Crystals

Photonic crystals are materials that are patterned with a periodicity in dielectric constant. They have a unique property of 'photonic band gap' i.e., a range of frequencies are forbidden to pass through the crystal. This implies that the photons with energies lying in the band gap are not allowed to propagate through the medium. This enables us to shape and mould the flow of light by engineering the crystal for the required application. The study of photonic crystals is analogous to semiconductors in solid state physics. This is depicted in **Fig. 1.2**.

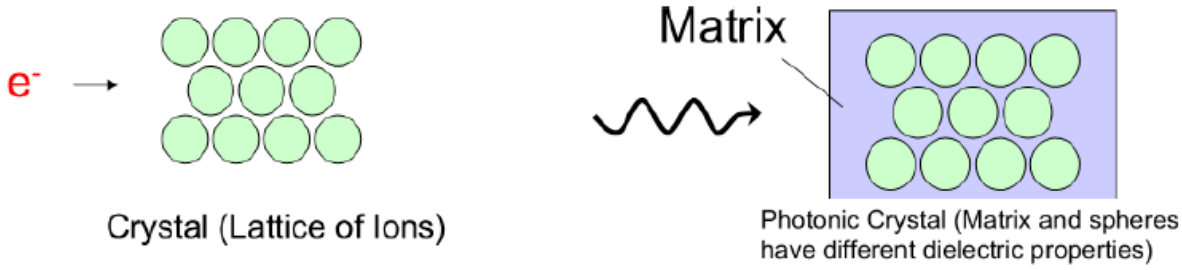


**Fig. 1.2:** Analogy of atomic lattice in a semiconductor and photonic crystal lattice [2]

In a semiconductor, the periodic lattice of atoms provides potential to the electron propagating through crystal. The geometry of atomic lattice and the strength of potential are such that the crystal shows an electronic band gap due to Bragg-like diffraction from the atoms i.e., there is a gap in allowed energies for which an electron is forbidden to propagate in any direction. Similarly in a photonic crystal,

the periodic lattice of macroscopic dielectric media provides to the photon propagating through crystal. If the difference in dielectric constants of constituent media is appreciable, then the phenomena of photons by Bragg scattering at the dielectric interfaces is similar to that of the electrons by atomic potential. This indicates that a photonic crystal can be designed in a way such that it possess complete photonic band gap i.e., a range of frequencies for which light is forbidden to travel in the crystal. By forbidden, it means that light can't travel unless there is a defect in the otherwise periodically patterned perfect crystal. In contrast to naturally occurring periodic arrangement of atoms in semiconductors, photonic crystals are artificially fabricated materials that are designed to exhibit periodic lattice. The challenge to fabricate these structures is that the lattice constant of photonic crystal (i.e., the size of the basic unit cell) must be comparable to the optical wavelength. These intricate structures are fabricated by microlithography techniques, such as electron-beam lithography and X-ray lithography [5].

### 1.2.1 Maxwell Equations in Photonic Crystals

In order to study the propagation of light in periodic dielectric media, we start the mathematical analysis by Maxwell's curl equations [1].

$$\nabla \times E + \frac{\partial B}{\partial t} = 0$$

$$\nabla \times H - \frac{\partial D}{\partial t} = J$$

$$\nabla . B = 0$$

$$\nabla . D = \rho \qquad (1.1)$$

where, E is the electric field measured in units of [volts/m] and H is the magnetic field, measured in units of [ampere/m]. The quantities D and B are the electric displacement and magnetic induction fields respectively. ρ and J are free charges and free currents respectively.

Quite generally in linear, isotropic and non-dispersive materials, the E and H fields are related to electric and magnetic flux through following equations:

$$D = \varepsilon E = \varepsilon_o \varepsilon_r E$$

$$B = \mu H = \mu_o \mu_r H \qquad (1.2)$$

where, ε and μ are the material's permittivity and permeability respectively.

We now make an assumption that there is no current flow or charge density in the system, therefore we get:

$$\nabla \mathrm{x}\, \mathrm{E} + \frac{\partial \mathrm{B}}{\partial \mathrm{t}} = 0$$

$$\nabla \mathrm{x}\, \mathrm{H} - \frac{\partial \mathrm{D}}{\partial \mathrm{t}} = 0 \qquad (1.3)$$

So,

$$\nabla \mathrm{x}\, \mathrm{E} = -\mu_{\mathrm{o}} \frac{\partial \mathrm{H}}{\partial \mathrm{t}}$$

$$\nabla \mathrm{x}\, \mathrm{H} = \varepsilon_{\mathrm{o}}\, \varepsilon_{\mathrm{r}} \frac{\partial \mathrm{H}}{\partial \mathrm{t}}$$

$$\nabla . \mathrm{H} = 0$$

$$\nabla . \mathrm{E} = 0 \qquad (1.4)$$

Normally, E and H are complex functions of space and time because the Maxwell equations are linear. However, by expanding the E and H fields into a set of harmonic-modes, the time dependence of fields can be separated from the spatial dependence. So the harmonic-mode is written as a spatial prototype or 'mode profile' times a complex exponential:

$$\mathrm{H}(\mathrm{r}, \mathrm{t}) = \mathrm{H}(\mathrm{r}) \mathrm{e}^{-\mathrm{i}\omega \mathrm{t}}$$

$$\mathrm{E}(\mathrm{r}, \mathrm{t}) = \mathrm{E}(\mathrm{r}) \mathrm{e}^{-\mathrm{i}\omega \mathrm{t}} \qquad (1.5)$$

By substituting equation (1.5) in equation (1.4), the two divergence equations give the conditions:

$$\nabla . \mathrm{H}(\mathrm{r}) = 0$$

$$\nabla . \mathrm{E}(\mathrm{r}) = 0 \qquad (1.6)$$

The two curl equations relate E(r) to H(r) as:

$$\nabla \mathrm{x}\, \mathrm{E}(\mathrm{r}) = -i\omega \mu_{\mathrm{o}} \mathrm{H}(\mathrm{r})$$

$$\nabla \mathrm{x}\, \mathrm{H}(\mathrm{r}) = i\omega \varepsilon_{\mathrm{o}}\, \varepsilon_{\mathrm{r}}\, \mathrm{E}(\mathrm{r}) \qquad (1.7)$$

For decoupling these equations, we divide the magnetic curl equation in equation (1.7) by $\varepsilon_{\mathrm{r}}$ and take the curl, as a result we get the following 'master equation'.

$$\nabla \mathrm{x} \left( \frac{1}{\varepsilon_{\mathrm{r}}} \nabla \mathrm{x}\, \mathrm{H}(\mathrm{r}) \right) = (\omega/c)^2 \mathrm{H}(\mathrm{r}) \qquad (1.8)$$

where, $\varepsilon_{\mathrm{r}}$ is the relative permittivity or, dielectric constant of media.

Equation (1.8) is an Eigen value equation that has the eigen value $(\omega/c)^2$ (where, $\omega$ is real i.e., lossless) and the Eigen operator $(\nabla \mathrm{x}\, 1/\varepsilon\, \nabla \mathrm{x})$ is the Hermetian operator. Here, H(r) represents the Eigen state, and the Eigen states are generally orthogonal. The two curls give us 'kinetic energy' and $1/\varepsilon$ gives us 'potential energy' [1].

### 1.2.2 Types of Photonic Crystals

Depending on the dimensionality of periodicity, photonic crystals can be categorized into one-dimensional (1D), two-dimensional (2D) and three-dimensional (3D) photonic crystals [1,5,26] as shown in **Fig. 1.3**. In 1D and 2D PhC, photons face band gaps only in the directions of periodic dielectric modulation. The propagation of em waves is not affected along the lattice directions that show no periodicity. One-dimensional (1D) photonic crystals are being used as mirrors in vertical cavity surface emitting lasers (VCSELs) from the time when the photonic crystals were not known. They are also known as the Distributed Bragg reflectors (DBR). They comprise of periodically patterned dielectric layers of different refractive indices. Two-dimensional PhCs have a periodicity of dielectric constant in two dimensions and are extended infinitely in the third dimension. They are engineered by periodically arranging air cylinders

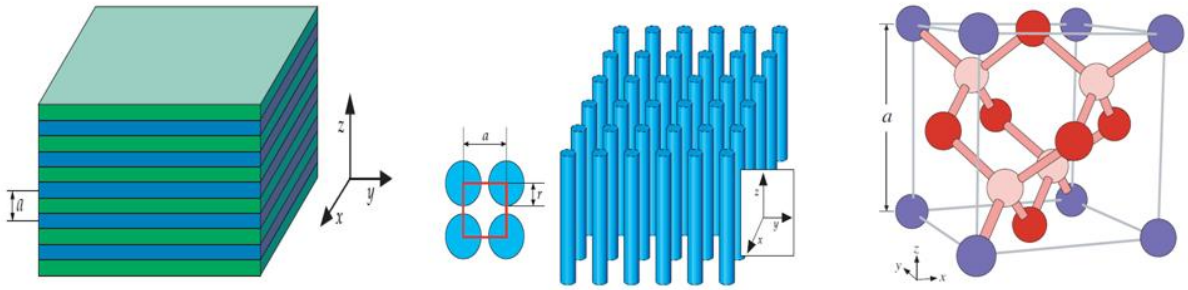


(a) (b) (c)

**Fig. 1.3:** (a) One- (b) Two- and (c) Three- dimensional photonic crystals. The defining feature of a photonic crystal is the periodicity of dielectric material along one or more directions [1]

in a dielectric material or dielectric cylinders in air organised in a square or triangular lattice. Three-dimensional PhCs are the pure photonic crystals in which light propagation is forbidden in all directions i.e., they can have a complete photonic band gap. Though, the propagation of light is controlled in all directions in 3D PhC's, their fabrication is still significantly challenging [5].

In this thesis work, 2D photonic crystal slab (also called quasi 3D photonic crystals) with triangular air-hole lattice is considered.

## 1.3 Photonic Crystal Slabs

Theoretically, the design of two-dimensional photonic crystals seems easy; however, they don't have simple fabrication procedure since they extend infinitely in the third dimension. Also, three-dimensional photonic crystals are very difficult to fabricate. To overcome this problem, the concept of 2D photonic crystal slab or quasi-3D photonic crystals was proposed [1,7,8,10,11,14,15,16]. This photonic crystal structure has received significant attention in recent years. The structure has a 2D photonic crystal lattice on a thin semiconductor slab with thickness of the order of one half of the optical wavelength i.e., $\lambda/2n$ , surrounded by air, as shown in **Fig. 1.4**.

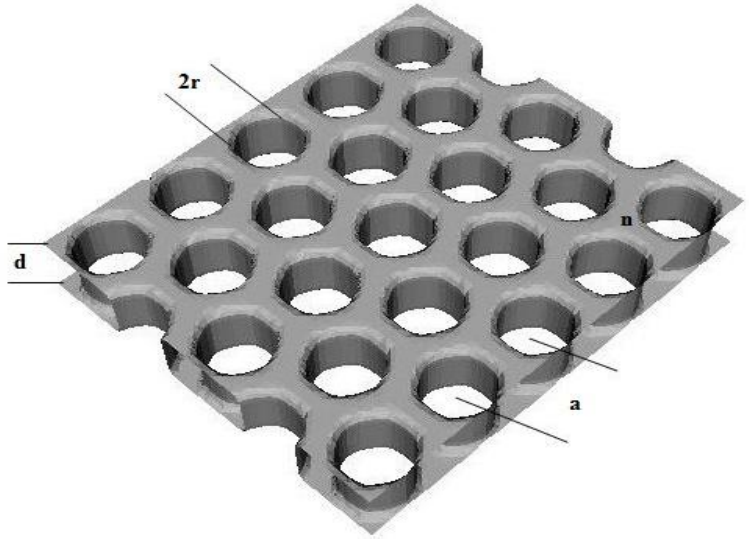


**Fig. 1.4:** Photonic crystal slab structure patterned with a triangular lattice, and the definition of its parameters (designed in MPB)

This structure retains most of the important features of 3D photonic crystal. The PhC slab structure can be fabricated easily, and is compatible with standard planar technology that is used to make electronic circuits. This is an appreciable advantage over 2D photonic crystals. When the photonic crystal slab structure is cladded by air in vertical direction on both sides, then it is termed as two-dimensional air-bridge photonic crystal [7]. The localization of light in PhC slab in three dimensions is made possible by a combination of two mechanisms. Light localization in the vertical direction is controlled by the Total Internal Reflection (TIR) as a result of high index contrast between the high-refractive index slab and the low-refractive index environment. The confinement of light in the lateral

direction is controlled by Distributed Bragg Reflection (DBR) as a result of 2D photonic crystal lattice. Since, light guiding in an air-clad dielectric slab depends on total internal reflection in the third dimension; therefore not all the modes are confined. There are both guided modes and leaky modes in the slab. At a particular constant frequency, there are a discrete number of guided field profiles or, modes. Each mode is expressed as the field distribution in the cross section orthogonal to direction of propagation and the in-plane wave number along the direction of propagation. The modes that have an in-plane wave number $k_{||} > \omega/c$ (where $c$ represents the speed of light in vacuum), satisfy the TIR condition and therefore, are confined in the slab. This principle is shown in **Fig. 1.5**. In this case, light can't couple out of the slab since the in-plane wave number is greater than the available wave number in air. The modes with in-plane wavevectors $k_{||} < \omega/c$ do not satisfy this condition and therefore, lie inside the light cone. A light cone is a cone which is represented by $k_{||} < \omega/c$ in the $\omega(k)$ presentation. A mode inside the light cone is extended in air and contributes to leakage of energy into the free space [8].

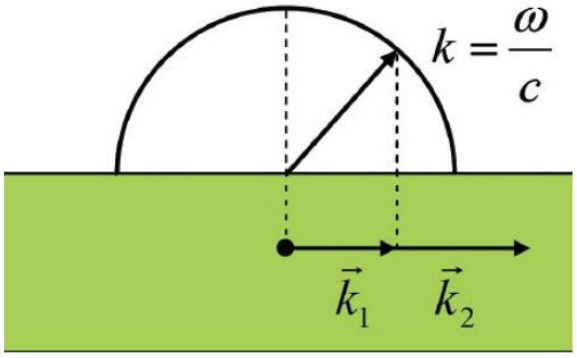


**Fig. 1.5:** Explanation of the light line concept for light guiding in the slab. A mode with a wave vector length $k_1 < \omega/c$ is not guided and can couple out in the air around the slab. A mode with $k_2 > \omega/c$ is guided and the total internal reflection condition is fulfilled because no corresponding wave vector with the same tangential component exists in air [8]

A complete photonic band gap does not exist in 2D photonic crystal slab because the radiative or leaky modes exist at all frequencies, even in the band gap region and these modes close the bandgap. However, the forbidden frequency range is still present for the guided modes of the slab. These guided modes are the photons that are confined in periodically patterned dielectric slab and decay exponentially into the cladding. This implies that the photonic band gap exists only for the guided modes of photonic crystal slab. The properties such as width and the position of the photonic band gap in two-dimensional photonic crystal slab (PCS) is dependent

on several important design parameters such as type of lattice (e.g., triangular, square), slab thickness, refractive index contrast between slab and cladding, lattice constant and holes radii (defined in **Fig. 1.2**). Therefore, by altering the size and periodicity of holes, it is possible to control the band-gap or tune the mirror properties of slab lithographically. This also reduces the fabrication complexity and cost of structure.

In 2D PhC, modes can be classified into two non-interacting classes of polarizations due to mirror reflection symmetry in the direction normal to the plane of periodicity. The two classes of polarizations are TE polarized modes with electric field in the plane of periodicity and TM polarized modes with magnetic field in the plane of periodicity. Similarly, guided modes in a photonic crystal slab can also be classified into two distinct classes. However, these modes are not purely TE and TM polarized in a photonic crystal slab because slab extends finitely in the vertical direction. Instead, they are decomposed with respect to a horizontal mirror plane bisecting the slab on the basis of whether they transform to be even or odd. These even and odd states resemble a lot with TE and TM modes respectively, in 2D photonic crystal. In fact, they are TE- and TM- like within the slab, and show a close similarity with the TE and TM modes in two-dimensional system [1,5,6].

Since the photonic band-gap in PCS depends on the type of lattice, researchers have found that a photonic crystal slab with triangular lattice has a much wider band gap than a square lattice because of greater symmetry and smoother Brillouin zone. Therefore, the triangular lattice is a more promising geometry comparatively for the realization of photonic crystal devices. Only TE-like eigen modes are of concern in triangular lattice photonic crystal slab [1,7].

## 1.4 Applications of Photonic Crystals

A photonic crystal provides us the capability to manipulate photons by engineering the structure accordingly and has received great attention in a variety of fields. By applying different types of engineering to the photonic crystal structure, photons can be manipulated in various ways. Band gap or defect engineering is one of the design criteria that focus on photonic band gap. To control light in various ways, one introduces into the crystal an artificial disturbance, or ‘defect’. By introducing line-shaped defects, an ultra-small waveguide can be formed that allows the light

transmission only along the defects. To form a photonic nanocavity, one introduces into the crystal point defects so that light can be trapped within the defect region. The combination of line and point defects find application in ultra small photonic circuits or chips with various functions. Moreover, the band gap helps to suppress spontaneous emission, which plays a major role in limiting the performance of various photonic devices. In a photonic crystal, one can also engineer the band edge, where the group velocity of light becomes zero. At the band edge, the light propagating in various directions combines by Distributed Bragg reflection to form a standing wave. With the use of this standing wave as a cavity mode, it is possible to realise a laser that enables coherent oscillation over a large 2D area. Furthermore, several types of novel nonlinear optical phenomena can also be possible with band-edge engineering. The other kind of engineering in photonic crystals is band engineering which focuses on the transmission bands that allow the propagation of light. By manipulating the dispersion relation obtained from the band structure, one can control the light in many ways. It is suggested that a variety of novel application and photonic devices can be developed for imaging by considerably slowing the propagation speed and by changing the propagation direction of the light in a photonic crystal, or by making negative refraction possible [9].

## 1.5 Thesis Objective

The objective of thesis is to design a nanocavity on photonic crystal slab with minimal out-of-plane and in-plane losses in order to achieve strong confinement i.e., ultra-high Q-factor and localization i.e., small mode volume of single mode within the cavity.

## 1.6 Format of Thesis

The thesis has been divided into five chapters.

1st Chapter provides a general discussion on photonic crystals, their analogy to semiconductors, Maxwell equations used to study electromagnetic wave propagation, different types of photonic crystals, concept of photonic crystals slabs and various applications of photonic crystals.

2nd Chapter provides an understanding of photonic crystal cavities, various types of cavities, key features of L3 PhC cavities and detailed explanation of the parameters quality factor and mode volume.

3rd Chapter provides a thorough review of literature on different types of photonic crystals, various photonic crystal cavities and optimisation of quality factor in cavities.

4th Chapter is about the analysis of photonic crystal cavity design. This chapter discusses the structure of photonic crystal nanocavity, MEEP simulation software for computational modelling, enhancement of Q-factor in the proposed cavity design, the methodology used and step by step design approach.

5th Chapter is the concluding chapter which summarizes the work and present its future scope.

# CHAPTER 2
# PHOTONIC CRYSTAL CAVITIES

## 2.1 General

Photonic crystal cavity is one of the most promising applications of photonic crystals because of their capability to confine light to small dimensions and volumes comparable to wavelength of light for long period of time [1,10]. A photonic crystal cavity can be created by introducing a point or line defect in the otherwise periodically patterned photonic crystal slab. As a result, the range of frequencies in photonic band gap that were earlier forbidden to travel in the photonic crystal slab can now be localised in the small region of defect. This happens because the symmetry of structure is tampered at the site of defect and the conditions of Bloch theorem are violated [11]. The cavity surroundings act as a perfect mirror and thus the modes at resonant frequencies are confined laterally within the cavity. A photonic crystal cavity can therefore be considered as an optical resonator [8]. The in-plane confinement of the modes is achieved as a result of Bragg's reflection by periodically patterned air holes in photonic crystal slab and vertical confinement is achieved as a result of total internal reflection at the slab-air interface. The nature of defect introduced in the photonic crystal is a key factor in controlling the shapes and properties of localised photonic states. The simplest form of photonic crystal cavity can be created by removing some of the dielectric material that should be present or by adding some of the dielectric material where it should not be there. This is termed as air-defect and dielectric-defect in the photonic crystal [5].Depending on the size of cavity, one can call a photonic crystal cavity as a microcavity if the size of cavity is in micrometer range; and a nanocavity if the size of the cavity is in nanometer range. The work in this thesis deals with photonic crystal nanocavities [12].

The confinement of light in PhC cavity is dependent on the wave vectors radiated vertically in the leaky region. The electric field inside the cavity is split into a set of plane waves with various wave vectors. The wave escapes from the cavity to the air clad around the photonic crystal slab only when the tangential component of

wavevector $|k_{||}|$ of each plane wave lies in the range 0 - $2\pi/\lambda$ (where $\lambda$ is the wavelength of light in air) because the conservation law for $|k_{||}|$ is satisfied at the air-clad interface. However, when $|k_{||}|$ is greater than $2\pi/\lambda$ then the light is confined strongly inside the cavity resulting in strong vertical confinement [7].The horizontal confinement of light can be achieved by increasing the number of photonic crystal layers around the cavity.

## 2.2 Types of Photonic Crystal Cavities

Broadly, photonic crystal cavity designs are categorized as:

- Hexagonal Cavities
- Linear Cavities
- Double Heterostructure Cavities

### 2.2.1 Hexagonal Cavities

The simplest type of PhC cavity is created by removing a single hole from the photonic crystal slab. This implies that a particular hole is filled with dielectric material of slab. Such a cavity design is termed as H1 Cavity i.e., hexagonal cavity with one layer of holes removed. **Fig. 2.1(a)** shows H1 Cavity with dielectric defect.

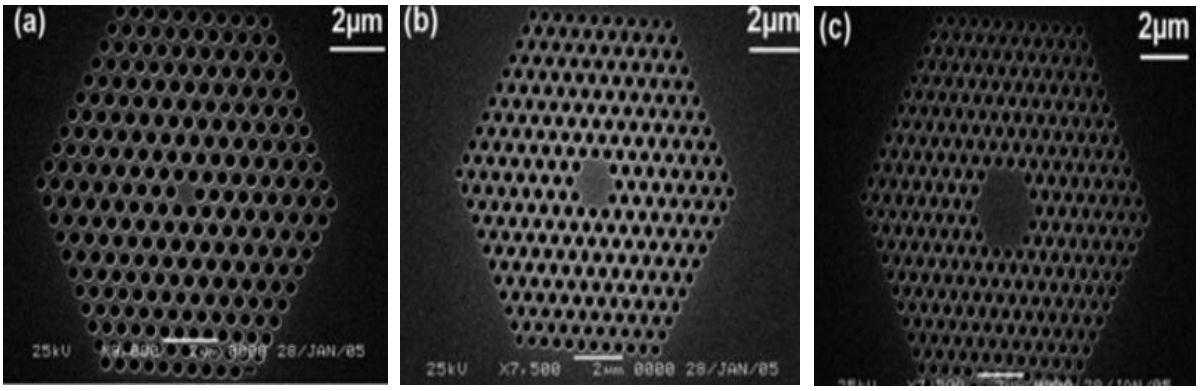


**Fig. 2.1:** Photonic Crystal Hexagonal Cavity (a) H1 (b) H2 (c) H3 [13]

The introduction of point defect (single hole removed) breaks the translational symmetry of photonic crystal and leads to strongly localized modes in the region of defect. These modes have frequencies in the photonic band gap and were earlier prohibited to travel in the PhC slab. Since the localized modes can't travel in the

periodically patterned photonic crystal surrounding the defect, they are spatially confined in the cavity. H1 Cavities normally show small mode volume and a low Q-factor. This indicates that such cavities have strong light localization but degraded quality. Other types of hexagonal cavities are H2 and H3 PhC cavities. H2 Cavity is formed by removing two layers of air-holes in hexagonal manner. This increases the size of cavity and results in better reflection of light at the site of the defect. Thus, H2 Cavities exhibit greater quality factor in comparison to H1 Cavities but at the cost of greater mode volume. **Fig. 2.1(b)** shows a H2 Cavity. Similarly, H3 Cavity can be formed by removing three layers of air-holes in a hexagonal manner. As a result, the size of cavity further increases. The localized modes now experience a better reflection from the PhC layer surrounding the defect. A better mirror reflection enhance cavity Q-factor but at the cost of further increase in mode-volume. **Fig. 2.1(c)** shows H3 PhC cavity design. Although Q-factor increases but the light localization degrades as we move from H1 to H2 and H3 PhC cavities. Generally, PhC cavity design is chosen on the basis of application requirement [14].

The most commonly used hexagonal cavity in recent literature is H1 Cavity because it has strong light localization and a small mode volume. Its quality factor is normally increased by shifting and shrinking first nearest neighbour air-holes surrounding the cavity. The orthogonally polarized doubly degenerate modes of H1 PhC cavity are used for wide variety of applications such as cavity-assisted generation of entangled photons, spin-photon media convertion, quantum information protocols and all-optical switches [15,16]. The hexapole mode of H1 PhC cavities is also receiving much attention because of its perfect hexagonally symmetric field distribution. The spatial symmetry of field reduces the vertical radiation loss because of destructive interference and far-field cancellation effects. Moreover, hexapole cavities can be easily coupled to a closely positioned waveguide or cavity and therefore, used extensively to form a coupled cavity system [17]. The small mode volume of H1 photonic crystal cavity finds applications in integrated lasers because the small mode volume lowers the threshold power required for pumping. H1 cavity is vertically coupled in most applications. The only limitation that H1 cavity shows is that of moderate Q-factor in comparison to linear and double heterostructure cavities [8].

### 2.2.2 Linear Cavities

Linear Cavities are formed by removing holes in a row instead of removing them in a hexagonal manner. The defect so formed is a thin region of dielectric material padded with periodically patterned air-holes all around. Ln defect PhC nanocavities show high Q-factor and small mode volume due to which it is one of the most widely accepted PhC cavity designs [18]. The localized modes in Ln cavity are similar to standing waves in a waveguide because the electric field decay exponentially at the cavity ends. Linear cavities can be coupled vertically and even sideways [8].

The commonly used linear cavities in recent literature are L3, L5 and L7 cavities. L3 Cavity is a linear cavity that is created by removing three air-holes in a row as shown in **Fig. 2.2** below. The orientation of electric field profile in L3 cavity is normal to the cavity axis and therefore cavity mode shows greater Q-factor as compared to H1 cavity.

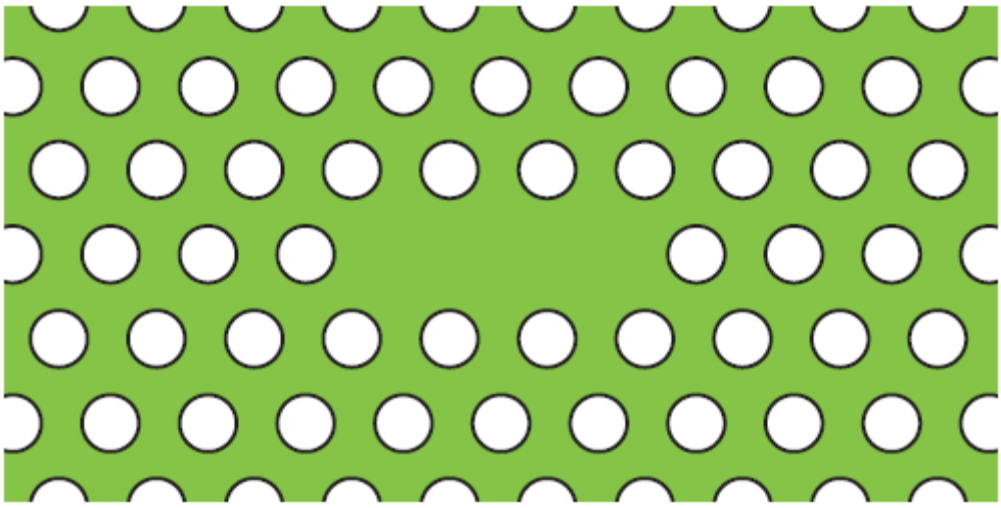

**Fig. 2.2:** Photonic Crystal L3 Cavity [8]

Similarly, L5 Cavity can be formed by removing five air-holes in a row as shown in **Fig. 2.3** below. The Q-factor in L5 Cavity is increased in comparison to L3 Cavities but the mode volume also increases which is not desirable. If we compare H3 and L5 Cavity designs, then L5 Cavity has a lower Q-factor due to small cavity size. However, the mode volume of L5 Cavity is smaller than H3 Cavity and therefore, it shows greater Q/V comparatively.

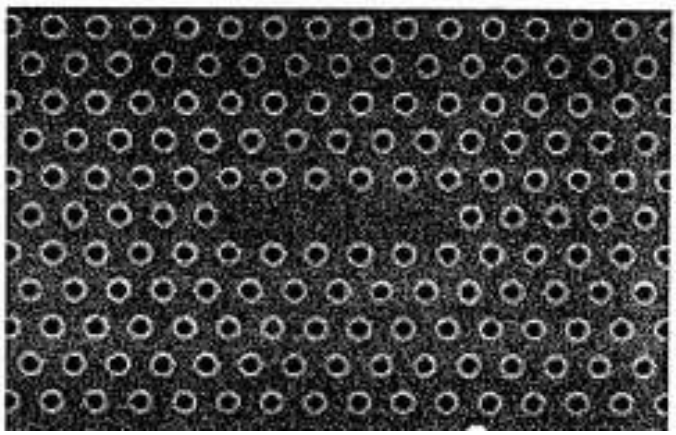

**Fig. 2.3:** Photonic Crystal L5 Cavity [19]

L7 Cavity can be formed in a similar fashion by removing seven air-holes in a row. The Q-factor increases further but at the cost of increased mode volume. L7 Cavity is as shown in **Fig. 2.4** below.

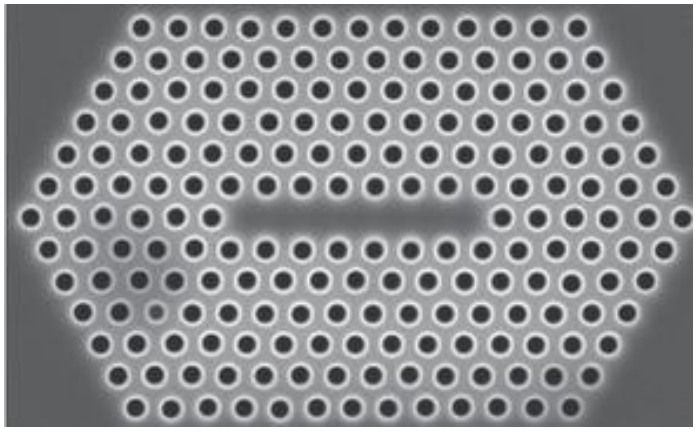

**Fig. 2.4:** Photonic Crystal L7 Cavity [20]

The variations in linear cavities are not similar to hexagonal cavities and therefore, properties shown by linear cavities differ as well. Linear Cavities show improved Q-factor and mode volume as compared to hexagonal cavities [6].

L3 Cavity design is one of the most popular PhC cavity structures due to its remarkable features. It has been reported that L3 cavity can easily give single mode that is strongly polarized even with large distortion in the photonic crystal design. This is in contrast to H1 PhC cavities that show split and nearly degenerate dipole and quadruple modes when the design is distorted. Moreover, the non-degenerate monopole mode and whispering gallery mode are also unsuitable since

they are unpolarized. It was also found that cavity modes in L3 Cavity are widespread and therefore, single mode can be selected easily [21].

Thus, L3 PhC cavities are better candidates than H1 Cavities in giving higher Q-factor and can even show single-photon emission. Due to this reason, L3 defect in PhC slab with triangular air-hole lattice is considered for thesis work.

### 2.2.3 Double Heterostructure Cavities

A photonic crystal heterostructure can be formed by joining two line defect waveguides in PhC with different lattice constant. Line-defect waveguide refer to missing air-holes in the entire row of PhC. A double-heterostructure PhC cavity is created by sandwitching a PhC line-defect waveguide with greater lattice constant between two PhC line-defect waveguides with a comparatively smaller lattice constant as shown in **Fig. 2.5**.

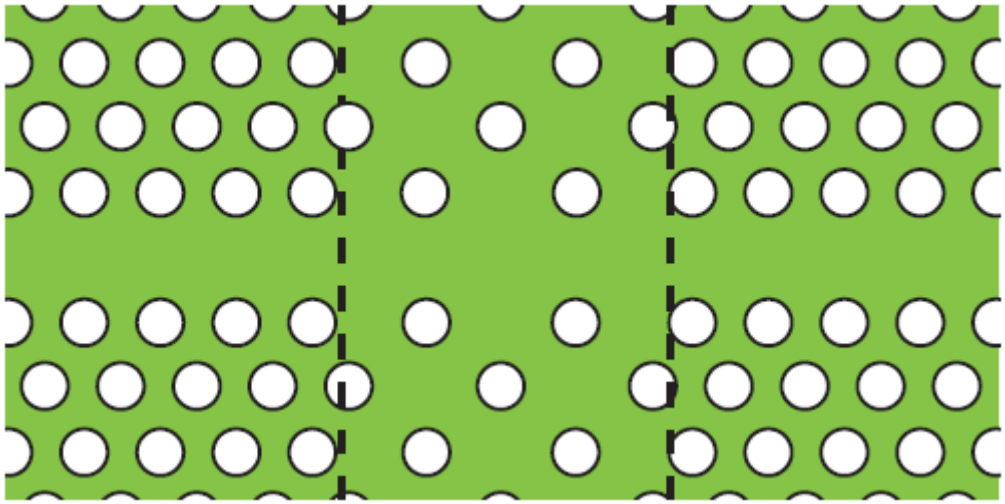

**Fig. 2.5:** Photonic Crystal Double Heterostructure Cavity. Green colour represents the dielectric material of slab and white colur represents the air-holes. The region between dashed lines forms cavity [8]

The PhC line-defect waveguide with smaller lattice constant has a guided mode with frequency in the photonic band-gap. During the transition, when lattice constant increases, the guided mode's frequency decreases. Therefore, in photonic double-heterostructure cavities, there exists a mode-gap, i.e., a frequency interval in which light can only travel in PhC with greater lattice constant. This implies that PhC line-defect waveguides with smaller lattice constant act as perfect mirrors to

the PhC cavity so formed in the central PhC line-defect waveguide with greater lattice constant. Usually, the difference between two PhC waveguides lattice constant is very small in order to reduce the out-of-plane losses, thus enhancing the Q-factor to a great extent [8,22]. Also, the central PhC waveguide which behaves as a cavity is usually taken of short length. A key-feature of photonic double-heterostructure cavity is the photon confinement due to mode-gap effect instead of photonic band-gap effect. The mode-gap effect is due to the lattice constant difference between two PhC waveguides [22]. These cavities can be side-coupled or transmission coupled [8].

## 2.3 Q-factor and Mode Volume

### 2.3.1 Q-factor

It has been mentioned earlier that light confinement in a photonic crystal slab is due to Bragg reflection in two dimensions and total internal reflection in the third dimension. This implies that horizontal confinement of light in cavity is due to photonic band-gap effect and its vertical confinement is due to total internal reflection. However, the defect modes in a cavity suffer from in-plane (horizontal) and out-of-plane (vertical) losses. A widely used parameter for the measurement of light confinement in cavity is Q-factor [1]. It is defined as the ratio of energy stored in the cavity to the power dissipated at center frequency. Englund *et al.* [29] derived an analytical relation between the quality factor and near field pattern of cavity mode, which is explained below:

$$Q = \frac{\omega U}{P} \tag{2.1}$$

where, ω is the angular frequency of the confined cavity mode.

The mode energy, U is given by the following expression:

$$U = \int \frac{1}{2} (\varepsilon E^2 + \mu H^2) dV \tag{2.2}$$

The calculation of far-field radiation intensity, P is complex.

In a two-dimensional PhC of finite depth, the in-plane ($P_{||}$) and out-of plane ($P_{\perp}$) mode loss mechanisms can be considered separately by the following expression:

$$P = P_{||} + P_{\perp} \tag{2.3}$$

The energy losses are inversely proportional to Q-factor [1]. Therefore,

$$\frac{1}{Q} = \frac{1}{Q_{||}} + \frac{1}{Q_{\perp}} \tag{2.4}$$

The light can leak laterally in the PhC slab if the number of photonic crystal layers around the cavity is finite. Lesser the number of PhC layers, more is the light leakage in the lateral dimensions. So, $Q_{||}$ which describes the lateral losses can be increased by increasing the number of photonic crystal layers around the cavity. The light losses in the vertical direction due to their coupling with the radiation modes that exist within the light cone in the background is described by $Q_{\perp}$ . The Q-factor is mainly determined by the energy losses due to the leaky modes that are radiated in the light cone since the energy losses in lateral dimensions can be controlled. Therefore, optimisation of vertical Q-factor is more significant. A suitable approach can thus be followed to reduce the wavevector components in the light cone in order to achieve strong light confinement in the cavity [8].

The near-field pattern at a surface S above the PhC slab contains the entire information about the out-of-plane radiation losses of the mode, and thus about $Q_{\perp}$. This means that we can estimate the radiated power and $Q_{\perp}$ from the known near field at the surface S.

The total time-averaged power radiated into the half space above the surface S is given by:

$$P = \int_0^{\pi/2} \int_0^{\pi} d\theta \, d\phi \sin(\theta) \, K(\theta, \phi) \tag{2.5}$$

where, $K(\theta, \phi)$ is the radiated power per unit solid angle. The radiated power per unit solid angle, K can be expressed in terms of 2D fourier transforms of $H_z$ and $E_z$ if we write the angles $\theta$ and $\phi$ in terms of wavevectors $k_x$ and $k_y$.

$$K(k_x, k_y) = \frac{\eta k_z^2}{2\lambda^2 k_{||}^2} \left[ \frac{1}{\eta^2} |FT_2(E_z)|^2 + |FT_2(H_z)|^2 \right] \tag{2.6}$$

In the above equation, $\eta = \frac{\mu_o}{\varepsilon_o}$ , $\lambda$ is mode wavelength in air, k= $\frac{2\pi}{\lambda}$ and $k_{||} = (k_x, k_y) = k(\sin\theta \cos\phi, \sin\theta \sin\phi)$ and $k_z = k \cos(\theta)$ denote the in-plane and out-of-

plane k-components, respectively. In Cartesian coordinates, the radiated power (2.5) can thus be re-written as the integral over the light cone, $k_{||} < k$. Substituting (2.6) into (2.5) gives

$$P \approx \frac{\eta}{2\lambda^2 k} \int_{k_{||} \le k} \frac{dk_x dk_y}{{k_{||}}^2} k_z \left[\frac{1}{\eta^2} |\mathrm{FT}_2(\mathrm{E_z})|^2 + |\mathrm{FT}_2(\mathrm{H_z})|^2\right] \quad (2.7)$$

Equation (2.7) gives the out-of-plane radiation loss as the light cone integral of the simple radiation term (2.6), evaluated above the PhC slab. Substituting Equation (2.2) and Equation (2.7) into Equation (2.1) yields a straightforward calculation of the Q-factor for a given mode. In the previous chapter, we discussed that we will be considering TE-like modes for triangular lattice photonic crystal slab. For such modes, the term $|\mathrm{FT}_2(\mathrm{H_z})|^2$ in (2.7) just above the slab is dominant, and $|\mathrm{FT}_2(\mathrm{E_z})|^2$ can be neglected in predicting the general trend of Q-factor.

### 2.3.2 Mode Volume

Another important parameter, that is used to quantify how well light is localised in the cavity is mode volume. The mode volume definition used in this work is in accordance to Purcell enhancement. Mode Volume ($\mathrm{V_{mode}}$) of cavity is defined as [23]

$$\mathrm{V_{mode}} = \frac{\int \varepsilon(\mathrm{r}) |\mathrm{E(r)}|^2}{\max(\varepsilon(\mathrm{r}) |\mathrm{E(r)}|^2)} \quad (2.8)$$

where, $\varepsilon(r)$ is the refractive index variation in space and E(r) is the electric field profile of the mode. A smaller mode volume is desirable in order to achieve strong light localization. The units of mode volume used in this work are $(\lambda/n)^3$ in relevance to Purcell factor, which is defined as [24]

$$\mathrm{F_P} = \frac{3}{4\pi^2} \frac{\mathrm{Q}}{\mathrm{V_{mode}}} \left(\frac{\lambda}{\mathrm{n}}\right)^3 \quad (2.9)$$

The above equation indicates that for spontaneous emission rate enhancement through Purcell effect, it is desirable to have maximal $\frac{\mathrm{Q}}{\mathrm{V_{mode}}}$.

## 2.4 Importance of PhC Nanocavities

High quality photonic crystal nanocavities that strongly confine photons in a small cavity region of optical wavelength dimension finds applications in various fields, such as photonics [3, 4, 14, 30], telecommunications [5, 6], quantum information processing [11, 15, 16] and cavity quantum electrodynamics [21, 37, 43] because a strong light-matter interaction is obtained. Photonic Crystal Nanocavities has gathered attention because of its potential of trapping and storing photons and enhancing light interaction with various functional materials and structures. The more the photon energy stored in the cavity, stronger is the light-matter interaction. Therefore, it is desirable to achieve ultra-high Q-factor and small mode volume. Some of the applications of photonic crystal nanocavities are low threshold LASER [14, 30, 38], photonic chips [6], atom trapping [22], bio-sensors [59], ultra-small filters [56], all-optical switches [58], single photon emitters [21], etc. . Kwon *et al.* [59] investigated photonic crystal cavities for enhancing the sensitivity to environmental changes and studied the resonance shifts due to refractive index change of the background material. He reported that the sensitivity of thinner slab with central air holes is 310nm/RIU (refractive index unit) and the sensitivity of heterostructure created in the slotted waveguide of thin PhC slab is 512nm/RIU owing to strong confinement of electric field in the low-index region. Takayagi *et al.* [15] reported on newly-designed H1-type photonic crystal (PhC) nanocavities that simultaneously exhibit high *Q* factors, small mode volumes, and high external coupling efficiencies of light radiated above the PhC membrane. He investigated dipole modes of the H1 PhC nanocavities, which are doubly-degenerate and orthogonally-polarized. Such nanocavities can be used in various potential applications, including cavity-assisted generation of entangled photons, spin-photon media conversion and all optical switches. Luxmoore *et al.* [37] explored the possibility of integrating single photon emitting III-V semiconductor quantum dots coupled to PhC nanocavities (made out of III-V material) on silicon substrate. He reported that III-V quantum emitters can be integrated on silicon platform for cavity-quantum electrodynamics. He suggested that with the addition of on-chip superconducting single photon detectors, all the elements required for scalable linear optical quantum computing can be combined in a single Si platform.

# CHAPTER 3
# LITERATURE SURVEY

**Yoshie *et al.*** [25] characterized donor-mode nanocavities formed by a single-defect cavity on photonic crystal slab having self-assembled grown quantum dots, emitting, in the range of 1.1-1.3 µm as luminescence sources. The nanocavity was created by replacing a large hole with a small hole at the center of thin slab of GaAs with triangular air-hole lattice. Fractional edge dislocation method was used to demonstrate the doubly-degenerate dipole states of cavity. The modification of the cavity design involved two important steps-(i) creating elliptical air-holes instead of circular air-holes in line with smaller hole in the x-direction. The major axis of the elliptical air-holes was elongated to 2r(1+ p/2$a'$) where r is radius of original hole and $a'$=$\sqrt{3}a/2$ is the original distance from vicinal lattice array in the y-direction, (ii) displacement of holes by p/2 from x-axis toward +y or –y direction. Samples with various p/a values and hole radii were fabricated and the dependence of p/a on photoluminescence spectrum was measured. It was observed that as p/a increases, a group of 'X' peaks above the SD1 resonance was more pronounced than the shift of SD2 resonance, i.e., fractional edge dislocation was more efficiently overlapped with SD1 mode. The behaviour of Q-factor and normalised resonance energy for different p/a values was analysed. It was observed that Q-factor increases as p/a increases where as resonance energy of SD1 mode decreases. SD2 mode was also observed to have the same frequency trend. It was found that the maximum quality factor of 2800 was observed at p/a=0.20 by luminescence from quantum dot emitters at 1.2 µm, where the PhC cavity design parameters are r=0.29a, $r'$=0.23a, d=0.65a. The results were verified through 3D-FDTD simulations that give Q-factor of 4400 and mode-volume of 0.43$(\lambda/n)^3$. It was reported that Q-factor values are higher than values of 1500 measured for donor mode cavities without fractional edge dislocation.

**Noda *et al.*** [26] investigated the effect of semiconductor 3D and 2D photonic crystals on the control of photons for possible applications to optical chip and functional devices. Full 3D photonic band gap crystals were created at near-

infrared wavelengths based on water-fusion and laser-beam assisted very precise alignment techniques. The clear attenuation of transmission was observed in 1.0-1.6 um wavelength region with maximum attenuation of -23 dB at 1.2 um(more than 99% attenuation) and the reflectance was observed to be 100% in same wavelength region. The effect of the introduction of a light emitter into 3D photonic crystal was also studied. The results (PL spectra) showed that the small number of stacking structures may well control (enhance and suppress) spontaneous emission. The design and fabrication of single-defect cavity in 3D PhC was also done and it was shown that the design of a defect with enough tenability, a large separation between first and second modes and a Q-factor of more than 5000 for small stacking numbers can be achieved. On 2D PhC's, a surface emitting type single defect channel drop filtering device was investigated. The device characteristics studied were Q-factor, drop frequency as a function of defect size, and in-plane to vertical coupling efficiency. A Q-factor of more than 400 was observed. The drop frequency was found to increase with an increase in defect size. The output efficiency is maximum (50%) when the energy flow of light from the waveguide through defect is optimal i.e., when $Q_{in} = Q_v$. The polarization characteristics were also described. The results indicated that polarization direction can be controlled by changing defect structure.

**Akahane *et al.*** [7] investigated light confinement in nanocavity surrounded by 2D PhC slab with a thickness of the order of wavelength of light to obtain high Q-factor and small mode-volume. It was found that the radiation loss at the edges of the cavity increases as the size of cavity decreases and therefore, Q-factor decreases. In order to suppress the radiation losses, a cavity structure was designed with three missing air rods at both edges in a 2D PhC slab. The electric field profile inside a cavity and its fourier transform before and after displacing the air rods at edges were studied. It was observed that the FT spectrum of the cavity with displaced air rods at edges has small components inside the leaky region. A number of samples with various air-rod shifts were fabricated and the resonant spectra of cavities were studied. It was observed that the width of resonant peak changes drastically with shift of air-rods. The minimum spectral width from the sample was 0.045 nm for air-rod shift of 0.15a, and a Q-factor of 45,000 was obtained. The

variation in Q/V values with the shift of air-rods was studied. Results indicated that a Q/V as large as $6.4 \times 10^{17}\, cm^{-3}$ can be achieved.

**Xiang-Hua *et al.*** [27] studied defect modes in a two-dimensional photonic crystal with deformed triangular lattice using FDTD method and supercell method. The behaviour of dipole-like defect mode in H1-defect PhC was investigated by stretching and shrinking the PhC lattice. As a result, a variation was observed in the frequency and magnetic field distribution of defect modes. It was observed that the doubly degenerate dipole modes can be separated to give a single mode emission for applications in PhC lasers. It was found that the cavities with shrinked lattice design are easier to fabricate and give strong localization of cavity modes in comparison to cavities with stretched lattice design. It was suggested that shrinking of lattice can be used to obtain single mode operation.

**Akahane *et al.*** [28] discovered a new design rule for L3-defect nanocavities in 2D PhC slabs in which six air-holes near the cavity edges are fine-tuned to give high Q-factor of 100,000 and mode volume 0.71 cubic wavelength. The idea behind this design is to reduce the out-of-slab light leakage in order to fulfil the TIR condition in the 3$^{rd}$ dimension of air-clad PhC slab. Therefore, appropriate hole-displacements were given to the first three air-holes on the cavity edges such that the envelope function of electric field profile in the cavity is spatially localised and has a gentle change at the cavity edges. This reduced the field components in the leakage region and subsequently enhances the Q-factor. Both FDTD simulation and experimental procedure were followed in order to determine the cavity Q-factor. The design parameters used were 2D PhC slab made out of silicon with triangular array of air-holes, lattice constant a=420 nm, radii of air-holes r=0.29a, slab thickness d=0.6a, slab index=3.4 and air-clad index=1. While simulating, first of all, outward displacements of 'A' air-holes (first nearest neighbour on cavity edge) was varied to study the variation in Q accordingly. Once, it is optimised, the outward displacements of 'B' air-holes (second nearest neighbour on cavity edge) was varied such that highest Q is achieved. Once 'A' and 'B' air-holes are optimised, finally outward displacement of 'C' air-holes (third nearest neighbour on cavity edge) is varied. The maximum Q-factor so obtained is 260,000 for A=0.20a, B=0.025a and C=0.20a.The mode volume remains constant despite air-

hole displacements and has a value 0.73 $(\lambda/n)^3$ at the final Q-factor. L3 PhC cavity was also fabricated to study the variation of Q-factor with the displacement of air-holes along the cavity edges. It was found that a maximum Q-factor of 100,000 can be achieved at A=0.176a, B=0.024a and C =0.176a. The mode volume calculated was $0.7(\lambda/n)^3$. The resonant spectrum obtained for optimised L3 cavity showed a narrow linewidth of 18 pm. It was concluded that the given L3 Cavity design shows a high Q/V of $1.4 \times 10^5 (\lambda/n)^{-3}$ which is larger by a factor of 16 in comparison to the L3 Cavity without air-hole displacements.

**Englund *et al.*** [29] discussed a general recipe for the design of 2D photonic crystal cavities with high Q-factor and small mode volume. This method overcomes the problem of parameter space search and lengthy trial and error optimisation of PhC cavities. An analytical approach is followed to find out the dielectric profile of cavity for the desired field distribution required to increase Q-factor with minimum mode volume. First of all, an expression was derived for out-of-plane radiation loss from PhC slab in terms of k-space distribution of cavity mode. Then, Q-factor was computed in terms of mode energy and far-field radiation intensity, derived earlier. Thus, an analytical relation between Q-factor and fourier transform of near-field pattern of the cavity mode was obtained. Next, a FT field pattern was chosen that gives the desired radiation losses. It was found that fourier transform of the mode should be centered at the extreme Brillouin zone to give minimum radiation loss inside the light cone and consecutively to achieve high Q-factor. Further, the variation of Q/V with mode volume was studied. It was observed that for a cavity mode with Gaussian distribution, Q/V increases exponentially with mode volume. For a cavity mode with sinc field envelope, it was found that a high Q/V can be achieved by eliminating the fourier components in the light cone. In the end, the approximate solutions were derived to find the dielectric profile of the cavity that supports the desired cavity mode. FDTD simulations were carried out for the derived Gaussian and sinc cavity that result in a high Q-factor of ~ $10^6$ and mode volume of ~ $(\lambda/n)^3$. It was concluded that the inverse approach to find out the cavity design is a rapid technique that results in a very large Q/V in single computational step.

**Song *et al.*** [22] proposed a photonic double heterostructure design in 2D PhC slabs in order to realise high Q-factor nanocavities that confine light in volumes of optical wavelength dimension. A 2D PhC slab was fabricated by joining two PhC to form a double heterostructure design. PhC 1 has a triangular lattice structure of lattice constant a1and PhC2 has deformed triangular lattice structure with lattice constant of a2 (a2 > a1) in the waveguide direction and a lattice constant of a1 in the orthogonal direction to satisfy lattice matching. Because of different lattice constant of PhC 1 and 2 in the waveguide direction, the transmission and mode gap regions of these PhC vary. The confinement of photons in the waveguide direction, as a consequence of mode-gap effect in the waveguide of PhC 1 leads to the formation of a nanocavity. This results in the possibility to control electric field confined in the PhC 2 into the waveguide of PhC 1, uniformly by changing the lattice constant difference between two crystals. The electric field distribution of a photonic double heterostructure cavity design and the cavity design with air-hole tuning were studied. It was observed that the electric field profile in the former case is more close to the ideal Gaussian curve. A tunable CW LASER was used as a light emitter to estimate the cavity Q-factor. The resonant spectrum of the cavity gives an extremely narrow linewidth of 2.8 pm. The intrinsic Q-factor obtained was $6 \times 10^5$ taking into account the effect of coupling between cavity and input waveguide.

**Chen and Towe** [30] proposed a methodology for achieving high Q-factor 2D photonic crystal slab defect cavities that allow current injection into their active regions. The proposed scheme combined the use of certain high-Q photonic crystal defect cavities with the technique of wet oxidation of (Al,Ga)As layers in the device structure. The photonic crystal chosen has a modified hexagonal lattice. The defect cavity was formed by removing one center hole in the hexagonal pattern, and at the same time reducing the diameter of six adjacent holes that surround it. The influence of high index substrate, top ohmic contact and the central electrical injection region on Q-factor was investigated through numerical simulations based on FDTD method. The high index of substrate tends to have deleterious effects on the cavity Q. The variation of of total Q-factor, vertical Q-factor ($Q_{\perp}$) and in-plane Q-factor ($Q_{||}$) as functions of normalised cladding thickness was analysed. The in-plane $Q_{||}$ doesn't change much where as the vertical $Q_{\perp}$ strongly depends on the

separation of high index substrate from the core-slab. Results indicated that the core-slab must be separated from substrate by low-index cladding with a minimum thickness of about 1.0a~1.4a, to prevent the degradation of Q-factor. The variation of Q-factor with different top cladding layer thickness was studied for drilling thickness of 2.8a and 3.5a. It was observed that the reduction in Q-factor with an increase in the thickness of top oxide cladding was not so dramatic when the deeper drilling depth used was 3.5a as compared to 2.8a. The calculations suggested that optimised Q-factor exist when the thickness of top contact layer is reasonably thick (0.20a-0.25a) for both drilling depths to ensure a good ohmic contact that readily promotes current conduction. The dependence of Q-factor on size of center opening was also studied. The Q-values appear to be insensitive to the size and existence of the center opening. However, it was found that if the center opening is too small, then the current may not be able to efficiently couple to the optical field to provide enough gain. Results showed that Q-factors of upto ~ $10^4$ can be obtained in structures with a realistic fabrication feasibility.

**Tanabe *et al.*** [17] studied the properties of hexagonal photonic crystal nanocavities based on a single point defect. The photonic crystal nanocavity was formed with a single missing air hole and by providing air-hole displacement to the first nearest neighbours. Both FDTD simulations and experimental work was carried out. It was found that the hexapole mode decreases the out of slab radiation because of destructive interference and far-field cancellation effects and results in an ultra high Q of $3.2\times 10^5$. It was observed that at a threshold power of 100 μW, cavity shows a bistable behaviour due to thermo-optic effect. The dynamic properties of the cavity were also studied and it was found that Q-factor decreases at higher input power.

**Tandaechanurat *et al.*** [31] analysed the dependence of Q-factor of dipole modes on slab thickness in H1-defect PhC nanocavities. It was observed that Q-factor of dipole modes increases by tuning slab thickness even after closing of photonic band gap between $1^{st}$ and $2^{nd}$ guided bands. These doubly degenerate and orthogonally polarized dipole modes in H1 Cavity were studied in detail by both 3D-FDTD simulations and practically through experiments. The research work was performed on a photonic crystal hole slab with refractive index 3.4 and H1-defect

formed by removing single hole from center. It was found that strong light confinement in the cavity is due to mode mismatching between guided modes and cavity modes. It was suggested that this finding can be applied to polarization entangled photon sources. It was reported that a high Q-factor of 16,200 can be obtained for a slab thickness of 1.35a.

**Fujita *et al.*** [32] discussed the emission of light in silicon with the use of photonic crystals and photonic crystal nanocavities. First of all, the optical emission properties of 2D PhC slab in Si were studied. It was observed that emission intensity is greater for photonic crystal samples as compared to non-photonic crystal samples. Further, it was observed that the emission intensity increases with an increase in the normalised frequency (lattice constant). It was reported that fabrication of photonic crystal structure has little effect on the quantum efficiency of silicon. The cavity modes of the nanocavity were analysed through FDTD simulations. The coupling efficiency for all the modes were calculated. It was found that only four of the six modes are visible in the spectra. Further, Q-factor of these four modes were calculated. The Q-factor of the lowest frequency mode is the highest with Q=1400. The observed emission intensity (L) for pumping at CW is expressed as

$$L = \eta_{ext} . \eta_c . \eta_i . V . J \qquad (3.1)$$

where, $\eta_{ext}$ is the light extraction efficiency, $\eta_c$ is the efficiency of coupling to objective lens, $\eta_i$ is the internal quantum efficiency, V is emission volume, J is pump density. The results indicated that emission intensity of Si is enhanced for each mode and it is associated with light extraction efficiency, which is determined by cavity Q and coupling efficiency. It was also reported that cavity mode wavelengths become longer with an increase in lattice constant. It was suggested that the internal efficiency of silicon can be improved further by controlling spontaneous emission in nanocavity.

**Notomi *et al.*** [33] demonstrated ultra high-Q and wavelength sized cavities using 1D photonic crystals for light confinement and compared them with 2D photonic crystals. Size modulated 1D stack cavity and 1D ladder cavity were examined. The dispersion relation of TE modes in line-defect in 2D triangular lattice air-hole

photonic crystal slab, 1D stack array waveguide and 1D ladder waveguide were studied. The theoretical Q and mode volumes obtained were Q=1.5 $\times 10^8$ and $V_{eff}$=1.5$(\lambda/n)^3$ for 2D PhC slab with line defect, Q=6.3 $\times 10^7$ and $V_{eff}$=2.1$(\lambda/n)^3$ for 1D stack array waveguide and Q=2 $\times 10^8$ and $V_{eff}$=1.4$(\lambda/n)^3$ for 1D ladder waveguide. The schematic and magnitude field distribution of 1D stack and 1D ladder waveguide were studied. The dependence of Q-factor and mode volume on cavity width and modulation depth was also studied. It was observed that for 1D stack waveguide, the mode volume decreases as the cavity width decreases, where as Q slightly increases from 4a to a and decreases at 0.75a. For 1D ladder waveguide, it was observed that Q also depends on depth of modulation and is maximum at around 20%. Mode volume slightly decreases as modulation depth increases. From the graphs, it was observed that $V_{eff}$ is 1.3 $(\lambda/n)^3$ and Q > $10^8$ when cavity width is 1a. It was found that 1D stack cavity is difficult to fabricate and 1D ladder structure is more realisable. It was concluded that 1D PBG cavities have the potential to replace 2D PBG cavities in many situations. Moreover, the simplicity in geometrical configuration and uniqueness of 1D PBG may open new possibilities for ultra high Q nanocavities.

**Deotare *et al.*** [34] investigated the design, fabrication and experimental characterization of high Q-factor 1D photonic crystal nanobeam cavities in silicon, operating near 1500 nm. The experiments were performed on a five-hole linear taper nanocavities in a free standing silicon nanobeam of thickness 220 nm and width 500 nm. The fabrication of the device was done on SOI substrate with a device layer of 220 nm and an insulator layer of 2 um. With the tapered mirrors designed to minimise reflection loss and precise control of cavity length, the theoretical Q-factors obtained for the cavities were as high as 1.4 $\times 10^7$. The fabricated devices were tested using a resonant scattering optical set-up and the cavity plays the role of wavelength selective polarization rotator in this scheme. The method proposed measures the intrinsic Q-factor of the cavity without loading effects due to the presence of coupling waveguides. The experimental results indicated that as the cavity becomes longer, the resonance should red-shift due to increase in the effective index of the cavity. The cavity Q-factor is modest (Q<10,000) for small and large cavity length, and shows a high value, Q=750,000 for cavity length of 146 nm. The resonant scattering spectra for a range of cavities

(s=116-117 nm) normalised by a background spectrum taken on the beam away from the cavity were studied. It was found that the cavities with higher Q were difficult to characterize using resonant scattering set-up because of the reduced contrast between resonant feature and coherent non-resonant background and the possible reason for this can be stronger photon confinement. The devices on silicon dioxide were also studied. The resonant scattering spectra for such devices show a moderate Q-factor of the order of $10^4$.

**Sweet *et al.*** [35] investigated the short-wavelength (~1000 nm) GaAs PhC slab nanocavities to study Q-factor. Many samples of GaAs nanocavities were grown and studied by atomic force, transmission electron, scanning electron microscopy and optical microscopy. It was found that the top of high Al-AlGaAs sacrificial layer in PhC slab nanocavities was rough inspite of the flat top surface of GaAs slab which leads to a decrease in Q-factor. The molecular beam epitaxy growth conditions were reported that reduce the AlGaAs roughness by an order of magnitude, but Q-factor is not much affected. It was demonstrated that a residue is left behind when the sacrificial layer is removed by hydrogen fluoride and potassium hydroxide can be used to remove this residue which results in a significant increase of Q-factor.

**Fan *et al.*** [21] investigated the properties of cavity modes in hexagonal-lattice H1 and L3 PhC slab cavities for applications in single photon emitters. Numerical simulations using 3D-FDTD method and experiments based on micro-photoluminescence measurements on fabricated GaAs PhC slab containg InAs quantum dots were carried out to compare H1 and L3 cavities. The lattice constant of 243-259 nm was considered for PhC cavities. The H1 cavity studied has six nearest neighbour air-holes shrinked and radially displaced outwards. The L3 cavity studied has elongated air-holes and two inner air-holes along the edges of defect shifted outwards. The mean length of major and minor axis of air-hole is d1= 178.8 nm and d2=153.4 nm. Design parameters of H1 PhC cavity chosen for study are d=1.13a, r=0.35a, $r'$=0.27a, $s_{H1}$=0.09a. Design parameters of L3 PhC cavity are r=0.32a, $s_{L3}$=0.17a. The electric field distribution of both cavities were obtained through FDTD simulations. H1 Cavity shows 6 modes that lie within the band gap (monopole, dipole, quadrupole and hexapole). The center frequency was

distributed from 0.2528 to 0.3112. The electric field distribution of L3 Cavity shows a fundamental mode at $f_{cn}$=0.2462 with Q=8.56 $\times 10^4$ and higher order modes ranging from $f_{cn}$ 0.2589-0.3149. The micro-photoluminescence measurements taken for H1 cavity reveals four peaks out of which only two peaks lie within the band gap. These 2 peaks represent orthogonally polarised x-dipole and y-dipole modes at 977.4 nm and 980.6 nm respectively and with Q-factors of 1200 and 1450 respectively. However, FDTD simulations carried out for H1 Cavity gives x and y-dipole modes at 962.2 nm with Q-factor of 8400. The deviation between simulation and experimental results is due to fabrication error in size and position of air-holes. The effect of tilting of air-hole sidewall by $1^o$ due to fabrication errors was also studied through FDTD simulations and it was found that Q-factor of x and y dipole modes drop to 3400 and center wavelength shift to 975.6 nm. This indicates the importance of verticality of air-hole sidewall in H1 cavities. The FDTD simulations were then performed for L3 cavities with approximate radius r= $\sqrt{d_1 d_2}/2$. Results show fundamental mode at 1051.8 nm and Q=2.71$\times 10^4$. The higher order modes for this cavity had short center wavelengths. At the same time, a distorted L3 cavity with elliptic cylinders was also studied. It was found that the frequency and Q-factor of the cavity modes for L3 Cavity doesn't vary much with distortion. The micro photoluminescence measurements carried out on L3 PhC cavities results in the fundamental mode centered at 996.2 nm and Q~2100. The variation in experimental and simulation value is due to fabrication imperfections and accuracy of calculation of FDTD simulations. For the same batch of samples of H1 and L3 cavities, it was observed that resonant frequency increase with r/a and period a. For the application of single photon emitters, a single mode must be obtained from a cavity. It was found that the degenerate dipole or quadrupole modes in H1 cavities split into doublet by fabrication errors. The non-degenerate monopole mode and whispering gallery mode are also unsuitable since they are unpolarised. Monopole mode can give a single mode but since it is unpolarised, it can't be used for single photon emitters. In contrast, it was found that L3 cavities can easily give a single mode and are strongly polarised. Moreover, the cavity modes are widespread and therefore, single mode can be selected easily. It was concluded that H1 Cavities exhibit split and degenerate dipole modes while, L3 cavities exhibit strong polarised single mode, even with

large distortion. Therefore, L3 Cavities are better candidates for single-photon emitters.

**Takayagi *et al.*** [15] proposed a design of H1 photonic crystal nanocavity that shows three properties simultaneously- high Q-factor, small mode volume and external coupling efficiency. Both FDTD simulations and experimental work was carried out to study the doubly degenerate and orthogonally polarised dipole modes in H1 PhC cavity. The investigations were performed on an air-suspended triangular-lattice hole slab made of GaAs (refractive index of 3.46) with a layer of InAs quantum dots in the middle. The cavity was optimised by changing the size and position of first nearest neighbour air-holes surrounding the cavity, changing the radii of second nearest neighbour air-hole in gamma-K direction and further providing hole-shift to third nearest neighbor in gamma-K direction. The design parameters used are lattice constant a=260nm, hole radii r=0.3a, slab thickness d=0.5a, first nearest neighbour hole radii=0.24a and hole shift=0.12a, second nearest neighbour hole radii=0.27a, and third nearest neighbour hole-shift=-0.26a. Negative sign here indicates that shift is provided inwards i.e., towards the cavity. It was found that cavity shows a Q-factor of 62,000, mode volume $0.47(\lambda/n)^3$ and coupling efficiency of 0.38 (assuming objective lens with moderate N.A. of 0.65) for the above design parameters. The near field distribution of cavity modes was also investigated in momentum space. It was observed that the ratio of leaky components to whole fourier components is reduced by 48% when the third nearest neighbour air-hole is provided a shift of 0.26a towards the cavity. This indicates a significant increase of Q-factor and coupling efficiency. By performing photoluminescence measurements, the results were experimentally verified. Experimental Q of 25,000 was reported for dipole modes. It was suggested that such a cavity can be useful in applications requiring vertical beaming of doubly-degenerate cavity modes.

**Hagameier *et al.*** [16] investigated H1 photonic crystal cavities for coupling of quantum dots to photons, that can find application in hybrid quantum information protocols. The aim was to achieve high extraction efficiency and Q-factor from the cavity design. The doubly-degenerate and orthogonally polarised dipole modes of cavity were considered for investigation. The design parameters are lattice constant

a= 260 nm, radius r=78 nm, membrane thickness d=130 nm, membrane (dielectric substrate) of refractive index 3.5 and an air-gap 'L' between membrane and bottom reflector. The far-field distributions were optimised by varying the sizes and positions of first nearest neighbour air-holes surrounding the cavity and by varying the air-gap between membrane and bottom reflector. It was reported that the given cavity shows a high Q of 15,000 and collection efficiency of 80% into an objective lens with N.A. 0.8. It was also found that the maximum mode matching of the device to a single mode fiber is 92%. It was suggested that such a design can be used for realising quantum information protocols.

**Pugh *et al.*** [36] demonstrated the effect of slab thickness in modified L3 defect thick photonic crystal slabs and discussed three confinement mechanism that can coincide to give high Q-factor when the conventional photonic band gap doesn't exist. The three confinement mechanisms discussed are- gentle confinement, guided mode overlap and vertical cavity resonance. Air-suspended photonic crystal slab made with AlGaInSb material with a high refractive index of ~3.8 and hexagonal array of air-holes is used for demonstration. The design parameters of PCS are r=0.35a, d=1.131a (1 μm), n=3.826 and lattice constant a=884 nm. The computations were performed by 3D FDTD method. The dispersion diagrams of PCS with slab thickness of 0.392a (400 nm) and 1.131a (1μm) were studied and it was found that the thick PCS (with slab thickness 1μm) doesn't show full guided mode band gap because the second guided mode was lowered. When L3 defect was introduced in thick PCS, two cavity mode resonances were found with the cavity. The cavity mode with higher frequency was studied in detail. L3 cavity was modified by displacing the air-holes on the edges of cavity to study the effect of gentle confinement in thick PCS. The variation of Q-factor for various hole shifts and slab thickness was analysed. It was found that for a hole shift of 0.14a, Q-factor increases suddenly from 2264 to 27661 in case of PCS with 1 μm slab thickness. This analysis proved the role of gentle confinement to increase the Q-factor without increasing the mode volume as it leads to lower field components in the light cone. To understand the role of guided mode overlap confinement mechanism, the electric field amplitude distributions in real space and k-space were studied. The PCS was excited by a broadband plane wave source outside the cavity. It was observed that there is a large peak in the center of light cone as equi-

frequency contour (EFC) of the light cone and the second guided Bloch mode were superimposed. This indicates that even though a strong in-plane PBG is absent in thick PCS, we can still obtain high Q-modes due to close proximity of EFC with light cone. The role of third confinement mechanism "vertical cavity resonance effect" was studied from the frequency snapshots taken off resonance for various hole-shifts. It was observed that the off-resonance vertical mode structure has a definite Fabry-Perot characteristic at the cavity center in case of 0.14a and 0.16a hole-shifts. This indicates that any electric field in light cone will resonate in the vertical direction leading to high Q-factor. The sudden drop of Q-factor from hole-shift of 0.14a to 0.16a was due to increased overlap of cavity-mode E-field and second guided Bloch mode in case of 0.14a hole-shift. It was concluded that the three confinement mechanisms can be combined to achieve high Q-factor in thick photonic crystal slabs.

**Kuramochi *et al.*** [18] proposed a new systematic hole-shifting rule in Ln photonic crystal slab nanocavities that can increase the Q-factor by an order of magnitude, both in theory and experiment in comparison to the conventional Ln design in which only two end-holes of the point defect are modified. The multi-hole shifting rule depends on two or three parameters. Three types of optimisation procedures were proposed. Type 1 optimisation involves initial inward shift of x~0.05a to A-holes and an outward shift of y to B and y/2 to C-holes (y~0.3a). It was observed that type 1 raises Q-factor by one order of magnitude in any Ln nanocavity (n>=1). However, it was found that Type 1 optimisation is sensitive to position error of air-holes surrounding D. So, Type 2 optimisation in which additionally, D-holes are given an initial inward shift of x/2 was considered as the correct design in comparison to type 1 optimisation. Both Type 1 and Type 2 optimisations were analysed numerically for Si PhC nanocavities by FDTD method. A more meaningful enhancement of Q-factor was found in Type 3 optimisation in which E and F holes are given an outward shift of z and z/2 (z~0.03a) in addition o e previous hole-shifts. Type 3 optimisation procedure was both numerically analysed and experimentally studied for InP nanocavities. The lattice parameters considered for numerical simulations were a=434 nm, r=100 nm, slab thickness=250 nm. The simulation results showed a high Q-factor of $2.2 \times 10^6$ and $3.3 \times 10^6$ for L3 and L5 nanocavities respectively. Type 3 Ln nanocavities were patterned on SOI wafers

for experiment. The experimental results obtained were Q=0.52 $\times 10^6$ for L2 and over $1\times 10^6$ for L3, L4 and L5 nanocavities respectively. The experimental result of Type 3 is considered for comparison. It was observed that the Q-factor increases by one order of magnitude in comparison to the conventional design. A key finding was that the x and y values determined by simulation can't be used for experiment. This was noticed when Q of $10^6$ was achieved for x=0.054a and y=0.280a instead of x=0.05a and y=0.3a for Type 3 L3 nanocavities. In particular, there was an error of 0.01a in y between simulation and experiment and this small change of y can decrease Q-factor by half. It was concluded that this new hole-shifting rule can improve the Q-factor in both homogeneous and buried heterostructure PhC slabs.

**Luxmoore *et al.*** [37] explored the possibility of integrating single photon emitting quantum dots coupled to III-V material for PhC nanocavities on silicon substrate. The high quality of III-V material for PhC nanocavities was demonstrated by the strong coupling regime. This indicated that III-V quantum emitters can be integrated on silicon platform. It was found that the challenge of coupling quantum light into Si photonic circuit can be overcome by lateral coupling of whispering gallery sources to silicon waveguides or, by epitaxial layer overgrowth. It was suggested that all the elements required for scalable linear optical quantum computing can be combined in a single Si platform, on the addition of on-chip superconducting single photon detectors.

**Saucer and Sih** [11] designed a new L3 photonic crystal cavity based on gravitational search algorithm that shows a remarkable Q/V of 798,000 $(\lambda/n)^{-3}$. This new design considers the modification of all the first nearest neighbour air-holes around the cavity. All the holes are allowed to vary in radii. Holes 'A' can move in the x-direction and holes 'B' and 'C' can move in both x and y directions. The parameter space involved 8 parameters $r_A$, $r_B$, $r_C$, $\Delta x_A$ , $\Delta x_B$, $\Delta x_C$ , $\Delta y_B$ and $\Delta y_C$. A new approach based on gravity and referred to as "Gravitational Search Algorithm" was used to fully explore the parameter space. These 8 parameters of L3 Cavity were considered as inputs to the fitness function i.e., Q/V ratio. FDTD simulations were used to calculate Q/V corresponding to each agent placed at a certain position. After a number of iterations, when the results converge, it was found that the new cavity design has Q-factor of 5,67,000 and mode-volume of

0.71 $(\lambda/n)^3$ i.e., a remarkable Q/V of 7,98,000 $(\lambda/n)^{-3}$. It was observed that GSA ran for 1.5 $\times 10^4$ FDTD simulations to fully explore the parameter space in comparison to $10^8$ calculations required otherwise. It was concluded that this nature inspired algorithm was useful in designing a new PhC cavity structure with high Q/V of 7,98,000 $(\lambda/n)^{-3}$.

**Lee** [38] investigated the mode-gap confined dielectric modes in 1D PhC NB nanocavities where PhC mirror with mode gap is formed by gradually increasing the lattice constant. The zeroth order dielectric modal properties were investigated and compared for two nanocavities N1 and N2 with different cavity sizes of $a_1$ and $2a_1$ respectively. It was observed that the threshold of N2 nanocavity (~350 uW) is smaller than that of N1 nanocavity (~460 uW) as $Q_{N_2} > Q_{N_1}$. Further, it was observed that the slope efficiency of zeroth order dielectric modes in N1 is greater than in N2 nanocavity as the dielectric mode in N1 nanocavity showed stronger vertically directional emission than that in N2 nanocavity. The results indicated that the lasing threshold and emission direction/intensity can be controlled by the modal symmetries. It was found that the lasing emission in N1 and N2 nanocavities are linearly polarised. A high Q of $3 \times 10^6$ and small mode volume of 0.39 $(\lambda/n)^3$ was obtained in case of N2 nanocavity. Rising of high order modes was observed for high Q-factor and it was indicated that to avoid the high order modes, the PhC mirror period should be sufficient to cause zeroth order dielectric mode lasing (n=8) and device footprint should be kept small (~15$\mu m^3$). 1D coupled NB nanocavities were also studied and it was shown that the bonding and antibonding modes in case of N2 nanocavity exhibit non-uniform mode distributions because of beamwidth mismatch between NBs. It was indicated that the mode field can be concentrated in either NB by spatially non-uniform carrier injection and thus, deciding and controlling the dominant lasing mode, and this can be used in switchable nanolasers.

**Sekoguchi *et al.*** [57] investigated absorption losses due to surface water adsorbed on the surface of Silicon heterostructure nanocavity. It was shown that the experimental Q-factor depends on ambient humidity, which is an indication that the absorption loss caused by surface water is significant. It was demonstrated that the absorption loss can be drastically reduced by applying chemical treatment to

remove thin $SiO_x$ layer at the surface. As a result, experimental Q-factor of 9 million was reported, which is the highest value yet for PhC cavities. Furthermore, the absolute value of absorption loss due to surface water was estimated with FDTD simulations, which clarify that the additional absolute Q-factor of about 7 million exists in standard Silicon high-Q nanocavities. The results represent great step toward an experimental Q-factor of more than 10 million and provide valuable information for the design of other Silicon photonics devices. It was indicated that these results provide important information for applications that utilize the surface such as sensors with high sensitivity.

# CHAPTER 4
# DESIGN AND ANALYSIS OF HIGH-Q PHOTONIC CRYSTAL CAVITY

## 4.1 Structure of Photonic Crystal Nanocavity

Researchers have found that even small modifications in the photonic crystal structure can result in a remarkable improvement of quality factor of the cavity [7, 30, 15, 18]. The objective of thesis is to optimise the structure of L3 nanocavity to achieve strong light-matter interaction i.e., ultra-high Q-factor and small mode volume of single mode localised in the cavity, that leads to a large Purcell factor.

A thin photonic crystal slab made out of gallium arsenide with a triangular array of air holes is considered for the research work. L3 type defect is created in the crystal with three missing air-holes in the center of the slab. The slab is air-cladded in the vertical direction in order to achieve Total Internal Reflection. With this structure, light can be confined by Bragg reflection for the in-plane directions. For the z direction, light is confined by the air clad [1,7].

The cavity structure is designed by shifting four nearest neighbour air-holes on cavity edges and shrinking first nearest neighbour air-holes. By shifting first nearest neighbour air-holes, we obtain a cavity mode with Gaussian electric field distribution as suggested in the reference 7. And, if we take the spatial fourier transform of electric field distribution inside the cavity, then we can analyse the wave-vector components in the light cone. The number of leaky wave-vector components is reduced when an optimum shift is provided to first nearest neighbour air-holes. By fine-tuning the three nearest neighbour air-holes on cavity edges, the electric field profile can be tailored and Q-factor can be increased [28]. Based on this concept, we further optimise the design by shrinking first nearest neighbour air holes on cavity edges. This results in an increase in Q-factor with minimal change in mode volume. We further provide displacement to fourth nearest neighbour air-holes on cavity edges. As a result, a large value of Q-factor and small mode volume is achieved for single mode in the cavity. This indicates that the mode is both temporally and spatially confined.

The dielectric profile of proposed L3 nanocavity design is as shown in **Fig. 4.1** in which the grey color signifies base material of PhC slab i.e. GaAs with refractive index 3.59 and white color signifies air with refractive index 1.

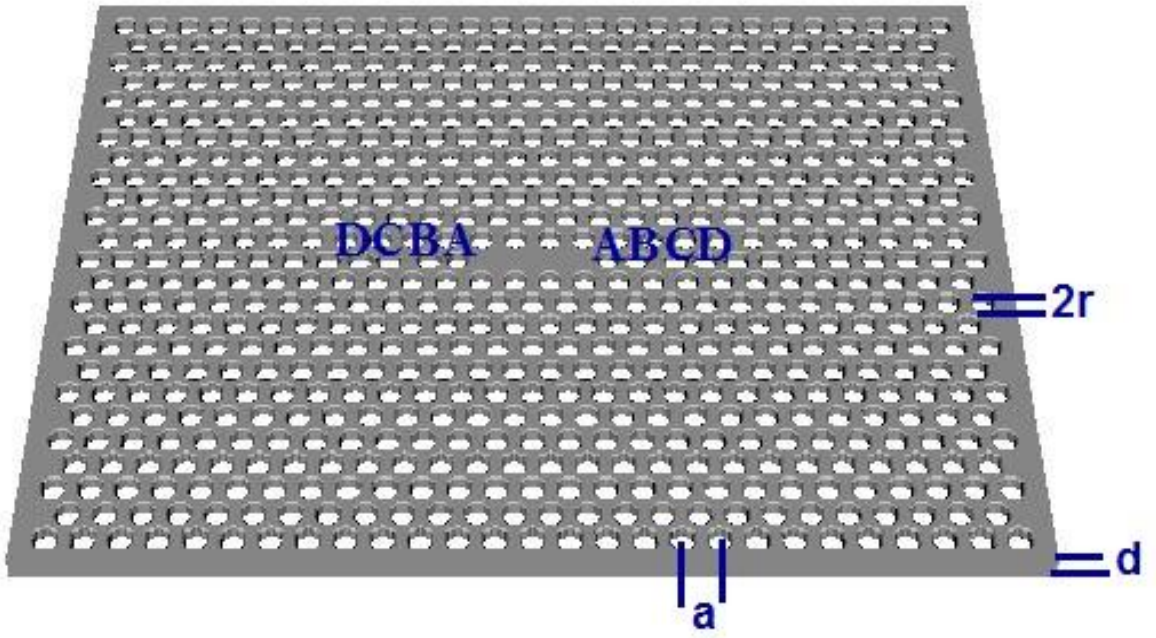


**Fig. 4.1:** 3D View of Dielectric profile of proposed high-Q L3 Nanocavity Design. Grey colour represents dielectric material (GaAs) of PhC slab. White colour represents air-holes. A, B,C,D are the four nearest neighbour air-holes on cavity edges that are fine-tuned. Lattice constant a=235nm, radii of air-holes r=0.3a, and slab thickness d=0.6a (designed in MEEP)

The two-dimensional view of the PhC nanocavity design is shown in **Fig. 4.2** below in order to have a better understanding of design parameters. The black color in the figure signifies base material of PhC slab i.e. GaAs with refractive index 3.59 and white color signifies air with refractive index 1.

The four nearest neighbour air-holes are denoted by A, B, C and D respectively. The air-hole displacements are provided in the outward direction of cavity as seen in the **Fig. 4.1** and **4.2**. The thickness of PhC slab, d is 0.6a and radii of air holes, r is 0.3a. There are twelve air-holes padded on each side of cavity. A perfectly matched layer of thickness 1a is taken at the ends of each dimension in order to avoid reflections. An air-clad of thickness 2a is taken in the vertical direction to achieve total internal reflection.

The air-hole displacements provided to four nearest neighbour holes on cavity edges are A-edgeshift=0.2a, B-edgeshift=0.025a, C-edgeshift=0.2a and D-edgeshift=0.05a respectively. The shrinked first nearest neighbour air-holes have

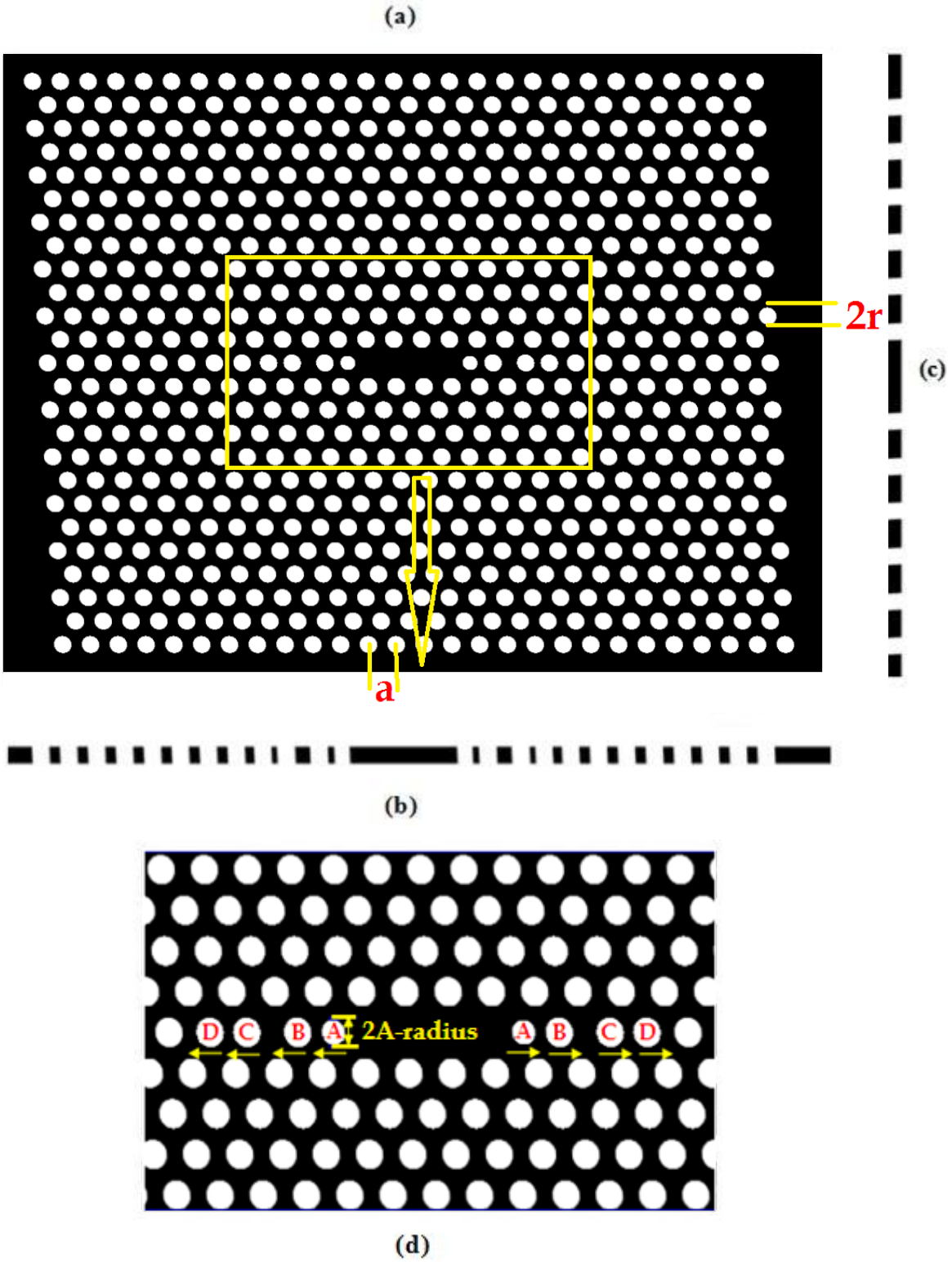


**Fig. 4.2:** 2-D View of Dielectric profile of proposed high-Q L3 Nanocavity Design in (a) x-y plane (b) x-z plane (c) y-z plane (d) Inset of fig. a that shows shifting of four nearest neighbour air holes on cavity edges and shrinking of first nearest neighbour air holes. The black colour represents the base dielectric material (GaAs) of PhC slab and white colour represent the air-holes. A, B, C and D represent the four nearest neighbour air-holes on cavity edges that are fine-tuned.

radii A-radius=0.25a. The length and width of cavity are 3.8a and 1.13a respectively. The computational modelling of the design is done in MEEP software.

## 4.2 MEEP for Computational Modelling of Cavity Design

MIT Electromagnetic Equation Propagation (MEEP) is a freely available simulation software package developed at Massachusetts Institute of Technology (MIT) to model electromagnetic systems. MEEP is based on finite difference time-domain (FDTD) method for computational electromagnetism in which space and time are divided into a regular grid, for solving Maxwell's equations in time domain. MEEP gives us an illusion of continuity. Even though the space is divided into a discrete grid and after that the fields are evolved in time using discrete time step, but as the grid and the time steps are made finer, a closer approximation for the true continuous equations is obtained. Many practical problems can be simulated essentially exactly. A common task in FDTD is to compute resonant modes or eigen modes of a given structure. For example, we can find out harmonic (definite-ω) modes at a given wavevector 'k' for a photonic crystal (periodic dielectric structure) or a waveguide or a resonant cavity that traps light in a small region for a long time. MEEP can calculate the decay time of cavity resonant modes and determine its quality factor Q. MEEP can quickly compute large numbers of modes at once by a single short pulse, and can efficiently extract modes in the interior of the spectrum (e.g. in a band gap). MEEP calculates all frequency modes at the same time, not consecutively [39, 40]. In this thesis work, MEEP software is used for the computational modelling of photonic crystal nanocavity.

## 4.3 Methodology for the design of Photonic Crystal Nanocavity

Researchers have tried a number of approaches to modify the design of photonic crystal cavity in an effort to further enhance the light-matter interaction. Some of them have shown improved Q-factor by elongating a line of air-holes using fractional edge dislocation [25, 43]. Some have varied the radii of a line of air-holes to improve Q-factor [29]. Others have modified the radii of air-holes on cavity surroundings [30]. Some researchers have even done a heuristic

optimization by replacing the round edge holes with very unusual designs [41]. The most common method of cavity optimization is that given in reference 7, in which two air-holes on the cavity edges are displaced in the outward direction.

As discussed in previous sections, there are energy losses in photonic crystal slabs as they show photonic band-gap effect in the lateral dimensions and not in the vertical dimension. These energy losses are quantified in terms of Q-factor. Q-factor is inversely proportional to energy losses. The energy losses in the plane of PhC slab are determined in terms of horizontal Q-factor and the out-of-plane energy losses are determined by vertical Q-factor. The horizontal Q-factor is affected by the size of the surrounding photonic crystal bulk and can be optimized by increasing the number of PhC layers. The optimization of vertical Q-factor is a serious task [1]. Numerous approaches have been proposed to reduce the out-of-plane losses from PhC slab. The simplest approach that is followed is the delocalization of cavity mode. In this approach, the mode volume of cavity is increased by reducing the energy inside leaky k-vector components. This is usually achieved by enhancing the length of defect in case of line-defect cavities [7] or by reducing the lattice constant mismatch in case of heterostructure cavities [22]. Large spatial distribution result in smaller wave vector spectrum and eventually reduces the number of wave vector components in the light cone. But, it is not desirable to have a greater mode volume in context to device miniaturization or in the applications that involve high optical field strengths. There is another way of minimizing the k-vector components inside the light cone by tailoring the symmetry of Fourier transform of field distribution of cavity mode. By choosing exact field distribution and size of defect, the defect modes that have odd symmetry with respect to planes normal to the direction of dominant contributions in Fourier space are created. As a result, such components are cancelled in the far field and hence, not radiated into the free space [8]. Apart from this, the shape of envelope function of cavity's mode can be altered. The field envelope that changes abruptly on cavity edges produce a broad intensity distribution in k space. This can be suppressed if we provide a more Gaussian-like field envelope. A proper modification of cavity structure can lead to Gaussian field distribution of cavity mode [42].

The design approach followed in this thesis work is based on the modification of the nearest neighbour air-holes of cavity in order to get Gaussian field distribution and reduce leaky wave vector components in the light cone. The cavity structure is designed in a manner to reduce the out-of-plane radiation losses and in turn, increase the quality factor of mode with not much variation in mode volume. Thus, the cavity mode will be gently confined and localized and a stronger light-matter interaction can be achieved. The analysis of photonic crystal is done in time domain and FDTD simulations are performed for computing resonant modes in cavity. In order to extract the frequencies and lifetimes (which may be infinite in a lossless system) with FDTD, the basic strategy is simple. First of all, PhC cavity structure with air cladding and absorbing boundaries is designed. Then the resonant modes of cavity are excited with a short pulse (broad bandwidth) from a current source that is placed inside the cavity. After the current source is turned off, some fields are bouncing around inside the system. The analysis of these fields is done to extract the frequencies and decay rates by filter-diagonalization method. Once the frequencies of cavity modes are known, the simulation is run again with a narrow-bandwidth (long-time) pulse so as to excite only the required mode. In order to find the cavity mode that has longest-lifetime, we run the simulation for long enough such that other modes decay away [40]. Hence, we get the resonant mode with maximum Q-factor in the nanocavity. After that, we study the field pattern of cavity's resonant mode and try to minimise the energy losses to achieve strong light confinement.

## 4.4 Enhancement of Q-Factor

The proposed design of photonic crystal cavity structure shown in **Fig. 4.1** is discussed in detail in this section. FDTD simulations are performed by placing a narrow-band source in the cavity to get the resonant mode with maximum quality factor. A single mode with resonant frequency 0.258 c/a and mode volume 0.8 $(\lambda/n)^3$ is obtained for the given design. The quality factor of the resonant mode is $4.93 \times 10^5$ and $Q/V_{mode}$ is $6.15 \times 10^5(\lambda/n)^{-3}$.

### 4.4.1 Analysis of Electric Field Distribution

The analysis of electric field distribution of cavity's resonant mode is done in MATLab. It can be seen in **Fig. 4.3** that the electric field profile of the designed cavity follows a Gaussian distribution. This indicates that the mode is gently

confined in the defect region and it plays a major role in the increase of Q-factor. The spatial fourier transform of electric field distribution of cavity's resonant

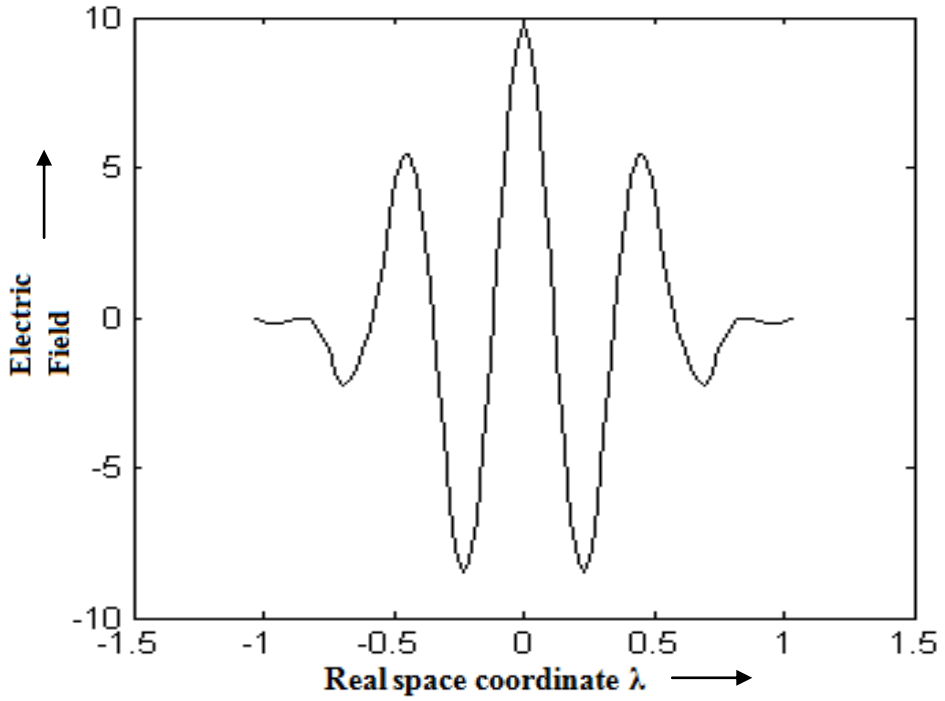


**Fig. 4.3:** Electric field distribution of confined cavity mode (designed in MATLab)

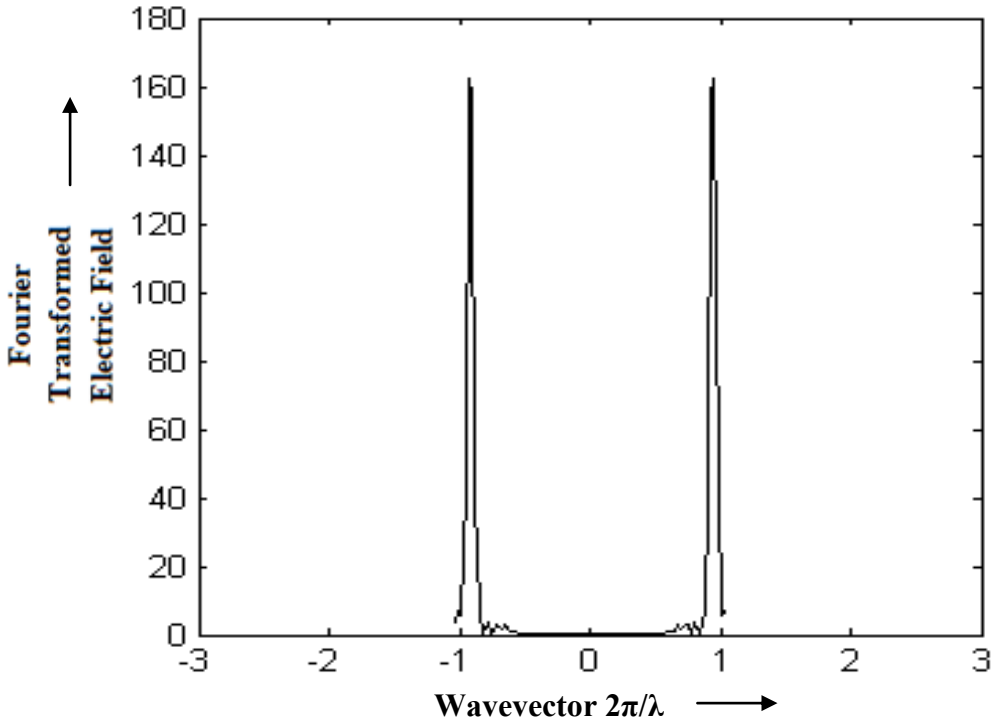


**Fig. 4.4:** Fourier transformed Electric Field of confined cavity mode (designed in MATLab)

mode is also studied. The fourier transform decomposes the electric field distribution into wave-vector components of plane wave and enables us to analyse the leaky wave-vector components in the light cone. It can be seen in **Fig. 4.4** that there are very few wave-vector components whose absolute value is in the leaky region of 0 to $^{2\pi}/_{\lambda}$. This indicates the ultra-high Q-factor of cavity mode.

### 4.4.2 Electric Field profile and Energy density

The electric field (Ey) profile of the resonant mode in cavity is as shown in **Fig. 4.5** .The L3 cavity shows a single mode with three anti-nodes, strongly confined and localised in the defect region. The electric field energy density of the confined cavity mode is as shown in **Fig. 4.6**.

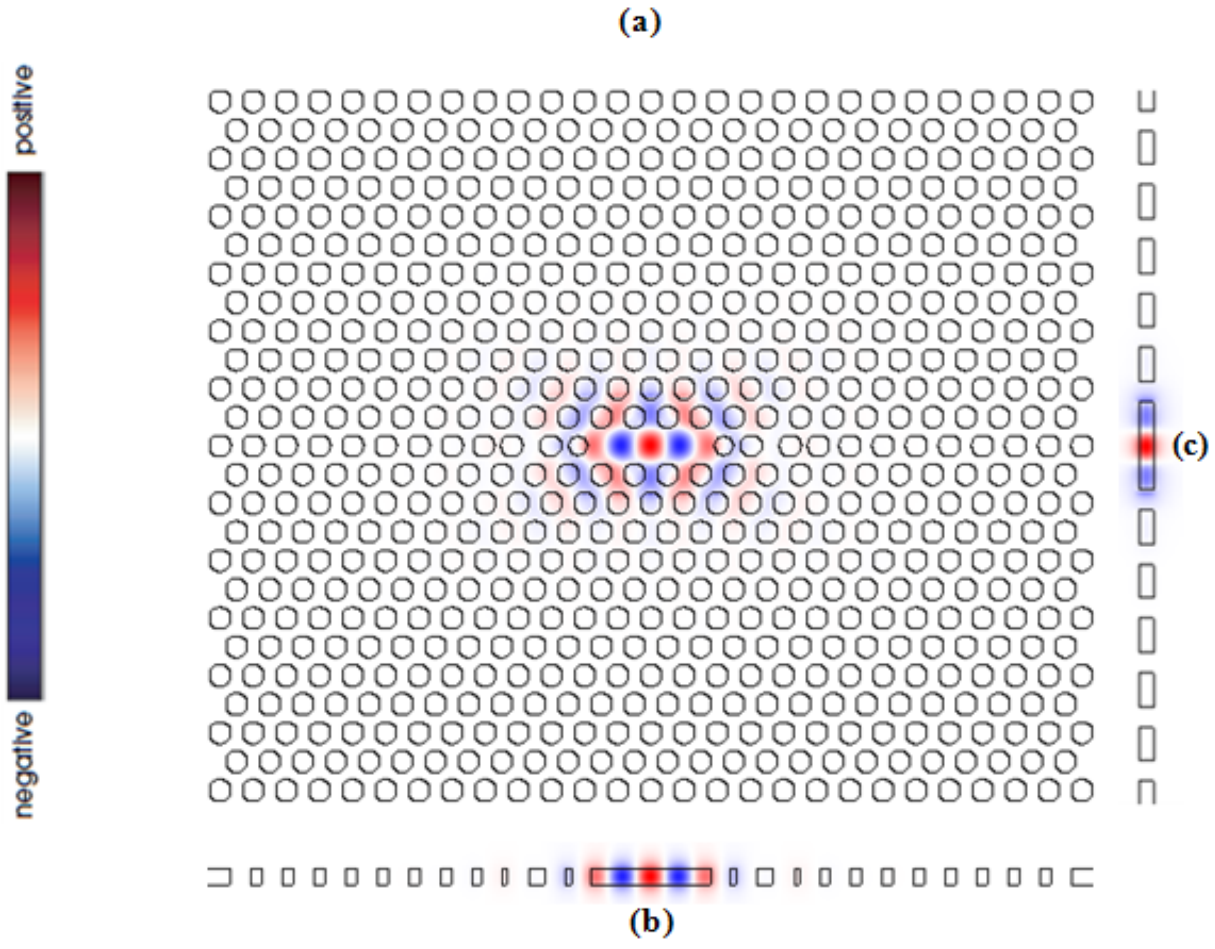


**Fig. 4.5:** Electric Field (Ey) profile of single mode confined in L3 Cavity in (a) x-y plane (b) x-z plane (c) y-z plane

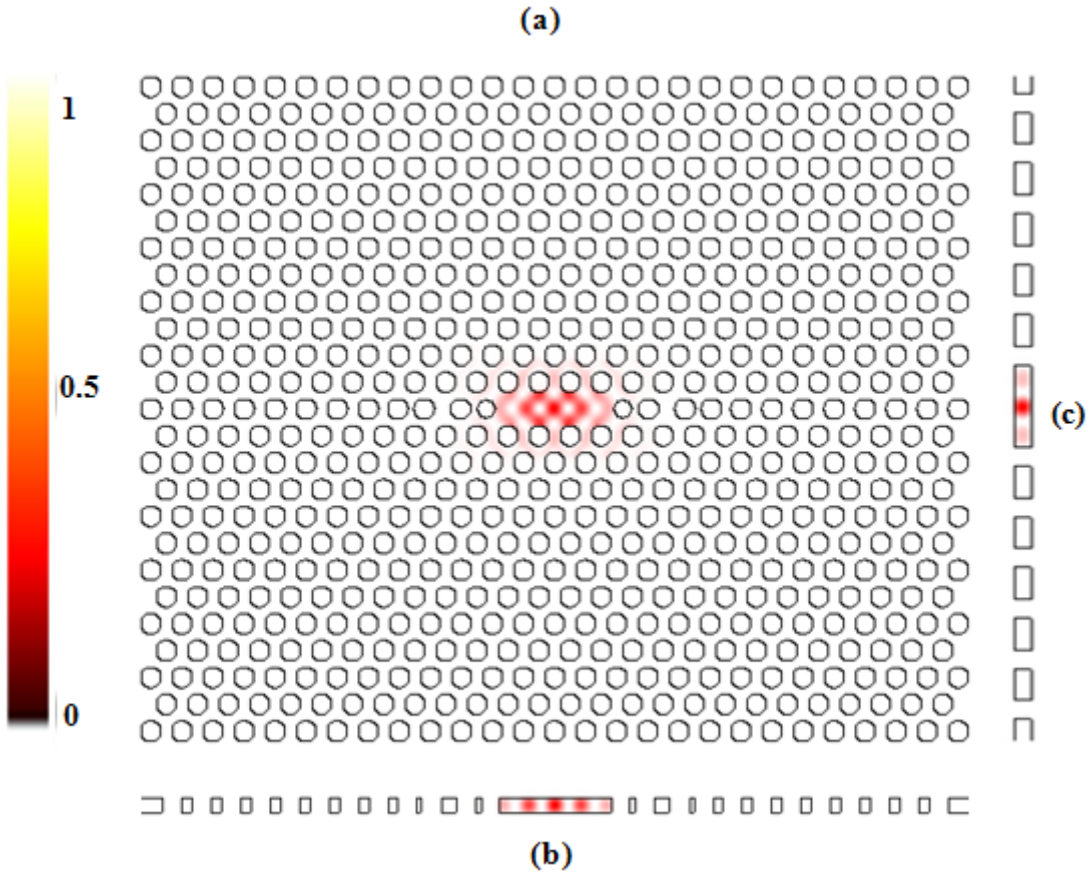


**Fig. 4.6:** Electric field energy density of confined cavity mode in (a) x-y plane (b) x-z plane (c) y-z plane

### 4.4.3 Design Approach

A step by step approach is followed for the given cavity design. **Table 4.1** shows the results obtained in each step.

**Table 4.1:** Step-by-step approach for L3 Cavity Design

| Design Parameters | | | | | Results | | | |
|---|---|---|---|---|---|---|---|---|
| **A-edgeshift** | **B-edgeshift** | **C-edgeshift** | **A-radius** | **D-edgeshift** | **Resonant frequency** | **Q** | **$V_{mode}$** | **$Q/V_{mode}$** |
| 0 | 0 | 0 | 0.3 | 0 | 0.263 | 5864 | 0.667 | 8783 |
| 0.2 | 0 | 0 | 0.3 | 0 | 0.261 | 134781 | 0.828 | 162740 |
| 0.2 | 0.025 | 0 | 0.3 | 0 | 0.261 | 157302 | 0.828 | 189938 |
| 0.2 | 0.025 | 0.2 | 0.3 | 0 | 0.261 | 339689 | 0.828 | 410235 |
| 0.2 | 0.025 | 0.2 | 0.25 | 0 | 0.261 | 413236 | 0.838 | 492574 |
| 0.2 | 0.025 | 0.2 | 0.25 | 0.05 | 0.258 | 493681 | 0.802 | 615152 |

Here, A-edgeshift, B-edgeshift, C-edgeshift and D-edgeshift signify outward hole displacements to first, second, third and fourth nearest neighbour on cavity edges respectively. A-radius signify the radius of first nearest neighbour on cavity edges. By optimising these parameters, Q-factor is enhanced. The mode volume remains less than 1 in the whole optimisation procedure. Finally, a high $Q/V_{mode}$ is achieved which results in Purcell enhancement and indicates a strong light-matter interaction. The units of resonant frequency, $V_{mode}$ and $Q/V_{mode}$ are c/a, $(\lambda/n)^3$and $(\lambda/n)^{-3}$respectively. The green background colour in table highlights the final results.

The approach followed for the proposed design of cavity is discussed step by step:-

**i) Enhancing Q-factor by shifting 1st nearest neighbour air holes on cavity edges**

First of all, the parameters Q-factor, $V_{mode}$ and $Q/V_{mode}$ are analysed for various air-hole displacements of 1st nearest neighbours on cavity edges. The behaviour of these parameters for various 'A' edge shifts is shown in **Fig. 4.7**. From **Fig. 4.7(a)**, it is observed that Q-factor increases as 'A' holes are shifted in the outward direction and attains a maximum value of 134781 for A-edgeshift of 0.20a and after that starts decreasing. This is a significant improvement of Q-factor from 5864 for no A-edgeshift. It can be observed from **Fig. 4.7(b)** that the mode volume doesn't show much deviation as we shift 'A' air-holes. It is varied from $0.667(\lambda/n)^3$ to $0.828\ (\lambda/n)^3$ while shifting 'A' air-holes by 0.20a. Though the mode volume increases, but still it is less than 1. It can be seen from **Fig. 4.7(c)** that $Q/V_{mode}$ shows a similar behaviour as Q-factor and increases to a value 162740 $(\lambda/n)^{-3}$ for A-edgeshift of 0.20a from 8783 $(\lambda/n)^{-3}$ for no A-edgeshift. The results indicate that shifting of first nearest neighbour air-holes by a small value of 0.20a can lead to a major improvement in the values of Q-factor and $Q/V_{mode}$. Hence, better light-matter interaction can be obtained.

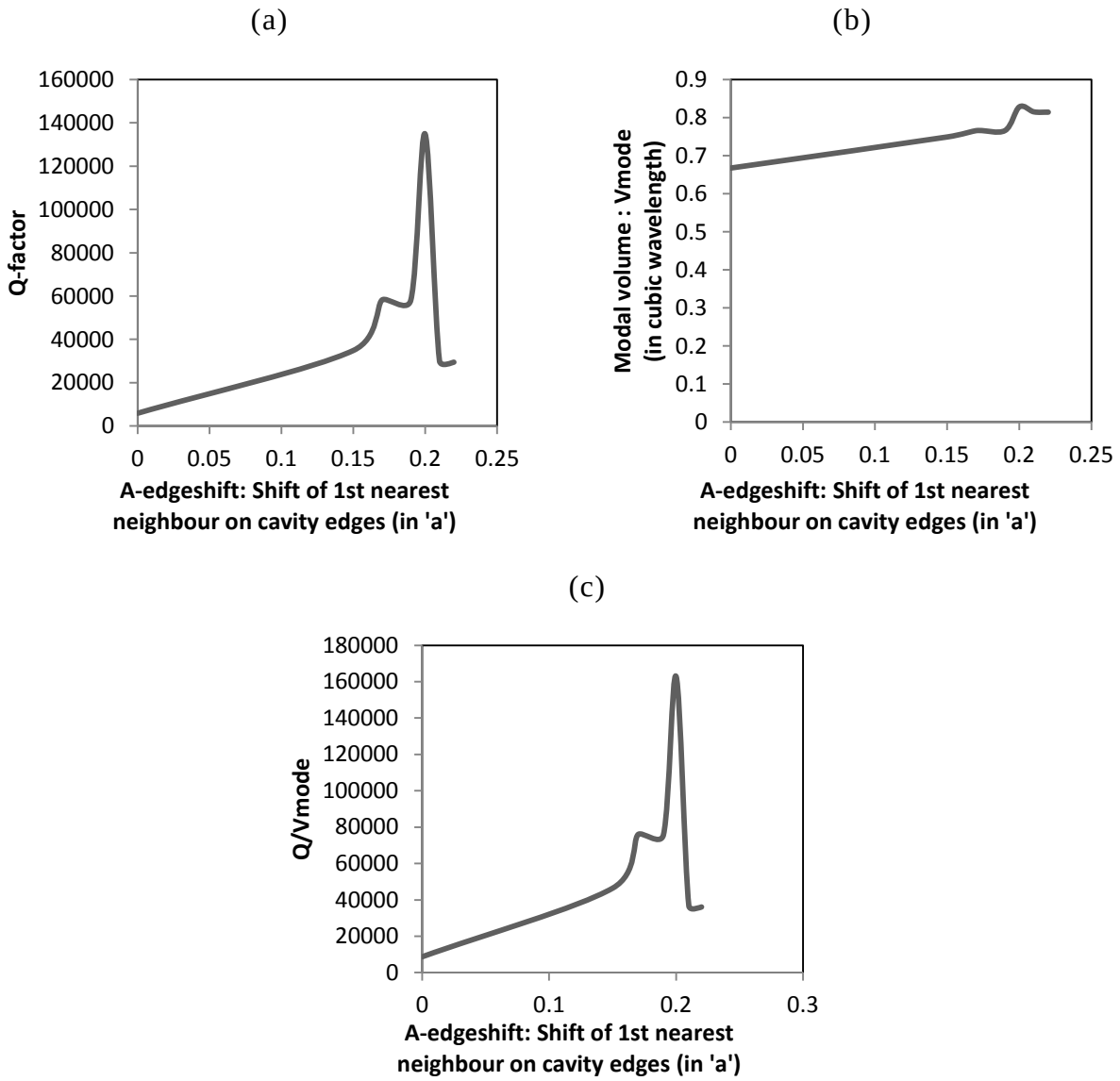


**Fig. 4.7:** Variation of (a) Q-factor, (b) $V_{mode}$ and (c) $Q/V_{mode}$ with 'A' air-hole displacements (maximum $Q/V_{mode}$ obtained for A-edgeshift of 0.20 with not much variation in modal volume)

**ii) Enhancing Q-factor by shifting 2nd nearest neighbour air holes on cavity edges keeping 1st nearest neighbour air hole displacement of 0.20a**

Next, the parameters Q-factor, $V_{mode}$ and $Q/V_{mode}$ are analysed for various air-hole displacements of 2nd nearest neighbours on cavity edges, keeping the shift of 0.20a of 1st nearest neighbours on cavity edges constant. **Fig. 4.8** shows the behaviour of these parameters for various 'B' edge shifts. Q-factor and $Q/V_{mode}$ both increase first as 'B' air-holes are shifted in the outward direction, reach a peak value and then decreases. From **Fig. 4.8(a)**, it is observed that Q-factor increases from 134781 for A-edgeshift of 0.20a to 157302 for A-edgeshift of 0.20a and B-edgeshift of 0.025a and after that starts decreasing. **Fig. 4.8(b)** shows that the

mode volume doesn't vary while shifting 'B' holes and is still $0.828(\lambda/n)^3$. From **Fig. 4.8(c)**, it can be seen that $Q/V_{mode}$ increases to a value 189938 $(\lambda/n)^{-3}$ and is a further improvement. Thus, it can be inferred that the displacement of two air-holes on cavity edges in the outward direction contributes in enhancing the parameters.

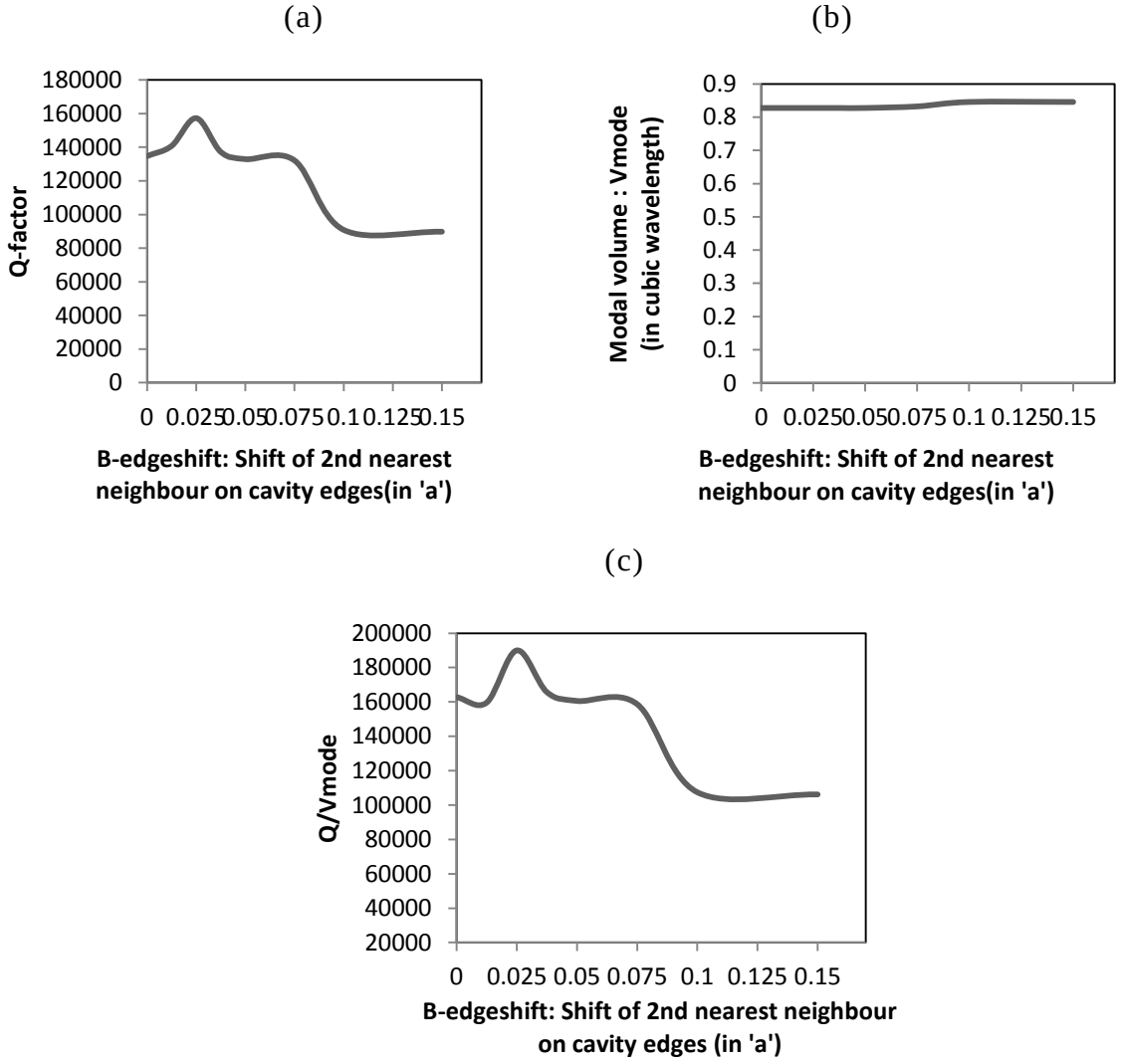


**Fig. 4.8:** Variation of (a) Q-factor, (b) $V_{mode}$ and (c) $Q/V_{mode}$ with 'B' air-hole displacements (maximum Q-factor obtained for B-edgeshift of 0.025 with not much variation in modal volume)

### iii) Enhancing Q-factor by shifting 3rd nearest neighbour air holes on cavity edges keeping 1st and 2nd nearest neighbour air hole displacement of 0.20 and 0.025 respectively

Next, the parameters Q-factor, $V_{mode}$ and $Q/V_{mode}$ are analysed for various air-hole displacements of 3rd nearest neighbour air-holes, keeping the shift of 0.20a of 1st

nearest neighbours on cavity edges and 0.025a of 2nd nearest neighbours on cavity edges constant.

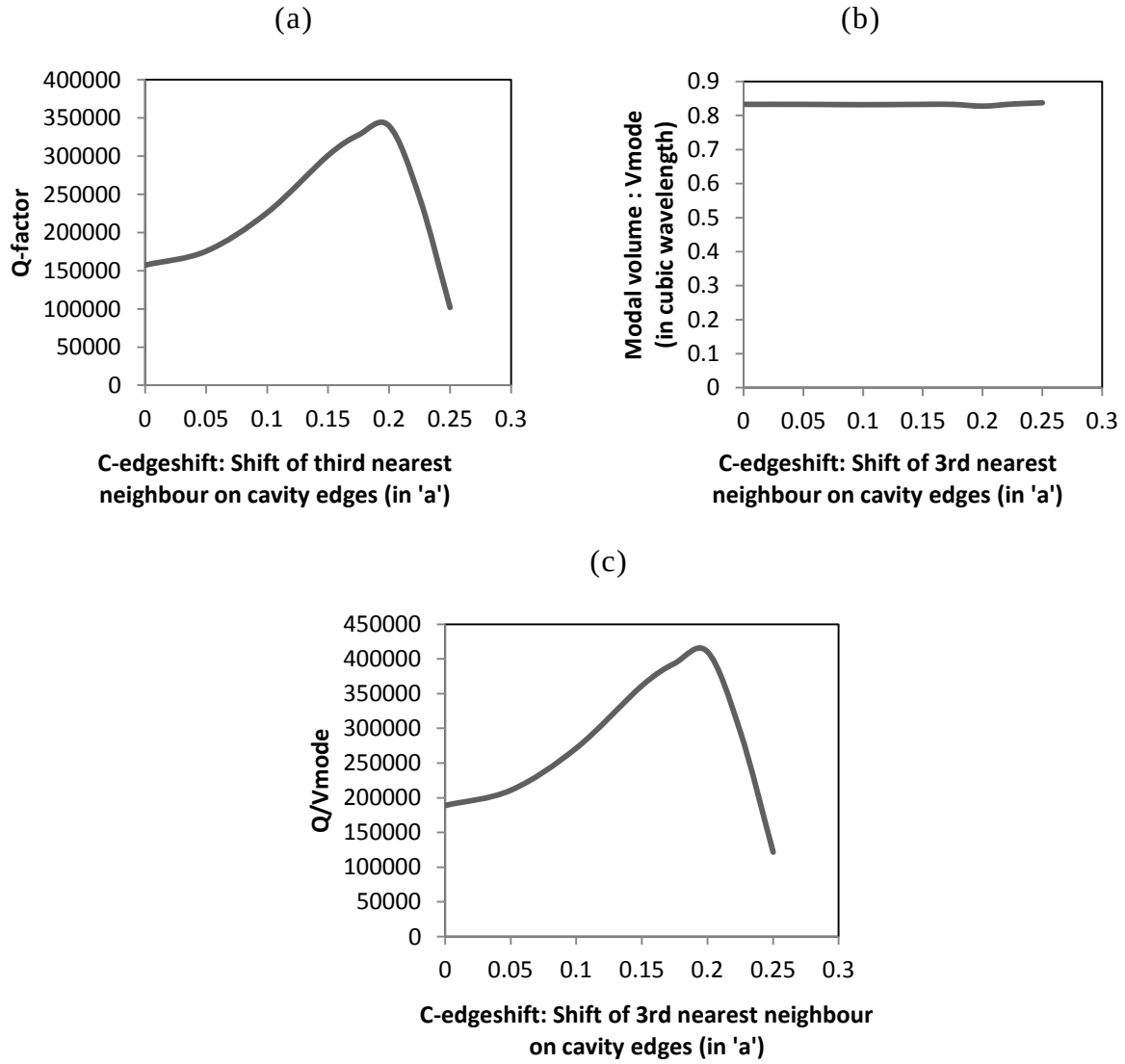


**Fig. 4.9:** Variation of (a) Q-factor, (b) $V_{mode}$ and (c) $Q/V_{mode}$ with 'C' air-hole displacements (maximum Q-factor obtained for C-edgeshift of 0.20 with not much variation in modal volume)

**Fig. 4.9** shows the behaviour of these parameters for various 'C' edge shifts. From **Fig. 4.9(a)**, it is observed that Q-factor increases from 157302 to 339689 for A-edgeshift of 0.20, B-edgeshift of 0.025a and C-edgeshift of 0.20a and after that starts decreasing. **Fig. 4.9(b)** shows that the mode volume doesn't vary while shifting 'C' holes and is still $0.828(\lambda/n)^3$. **Fig. 4.9(c)** shows that $Q/V_{mode}$ increases to a value $410235(\lambda/n)^{-3}$ and is a great improvement. As a result of shifting three nearest neighbour air-holes in the outward direction, Q-factor and $Q/V_{mode}$ shows a much higher value in comparison to the unoptimised cavity.

**iv) Enhancing Q-factor by shrinking 1st nearest neighbour air holes on cavity edges keeping 1st, 2nd and 3rd nearest neighbour air hole displacement of 0.20, 0.025 and 0.2 respectively**

(a)

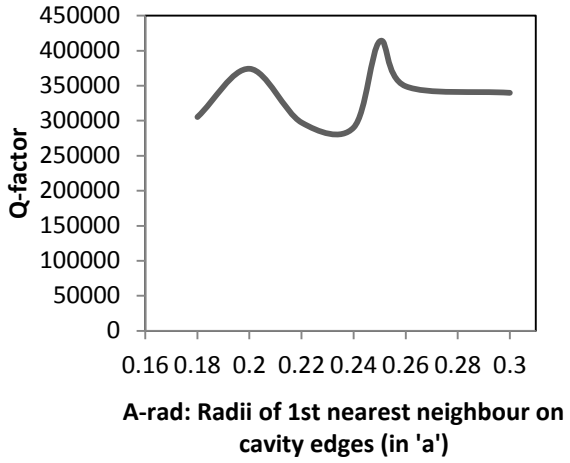


(b)

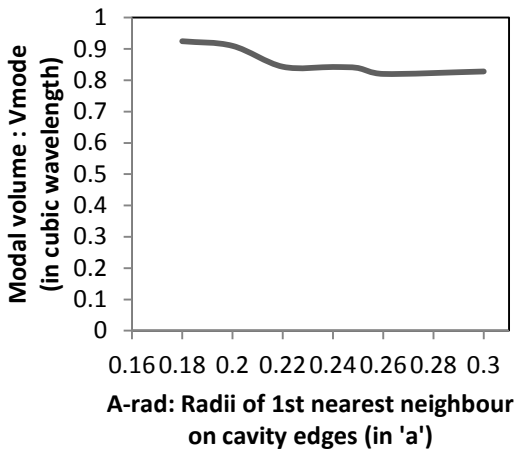


(c)

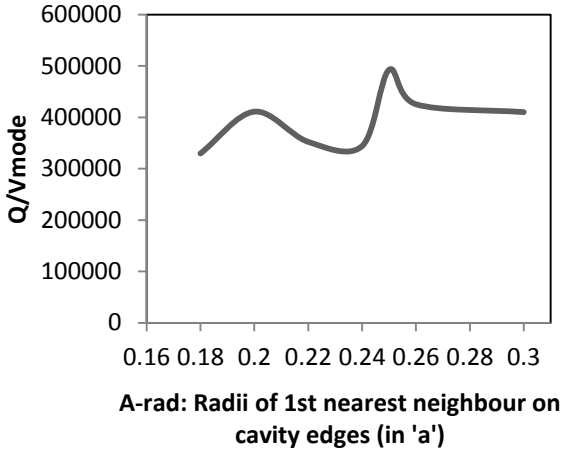


**Fig. 4.10:** Variation of (a) Q-factor, (b) $V_{mode}$ and (c) $Q/V_{mode}$ with 'A' air-holes radii (maximum Q-factor obtained for A-radius of 0.25 with not much variation in modal volume)

In an endeavour to achieve better results, we shrink the first nearest neighbour air-holes on cavity edges. **Fig. 4.10** shows the behaviour of these parameters for various 'A' holes radii. Q-factor and $Q/V_{mode}$ show an initial increase and then decrease. From **Fig. 4.10(a)**, it is found that Q-factor shows a further improvement from 339689 to 413236 for A-rad=0.25a. **Fig. 4.10(b)** shows that the mode volume doesn't vary while shrinking 'A' holes and is still $0.828(\lambda/n)^3$. From **Fig. 4.10(c)**, it is observed that $Q/V_{mode}$ increases to a value $492574(\lambda/n)^{-3}$ from $410235(\lambda/n)^{-3}$. This shows that the shrinking of 'A' air-holes plays an important role.

**v) Enhancing Q-factor by shifting 4$^{th}$ nearest neighbour air holes on cavity edges keeping 1$^{st}$, 2$^{nd}$ and 3rd nearest neighbour air hole displacement of 0.20, 0.025 and 0.2 respectively and 1$^{st}$ nearest neighbour air hole radii of 0.25**

Finally, we shift the fourth nearest neighbour air holes and analyse the parameters Q-factor, $V_{mode}$ and $Q/V_{mode}$. **Fig. 4.11** shows the behaviour of these parameters for various 'D' air-hole shifts. **Fig. 4.11(a)** shows an improvement in Q-factor is observed from 413236 to 493681. The mode volume doesn't vary while shifting 'D' holes and is still $0.828(\lambda/n)^3$ as seen in **Fig. 4.11(b)**. **Fig. 4.11(c)** shows that $Q/V_{mode}$ is increased to $615152(\lambda/n)^{-3}$ from $492574(\lambda/n)^{-3}$.

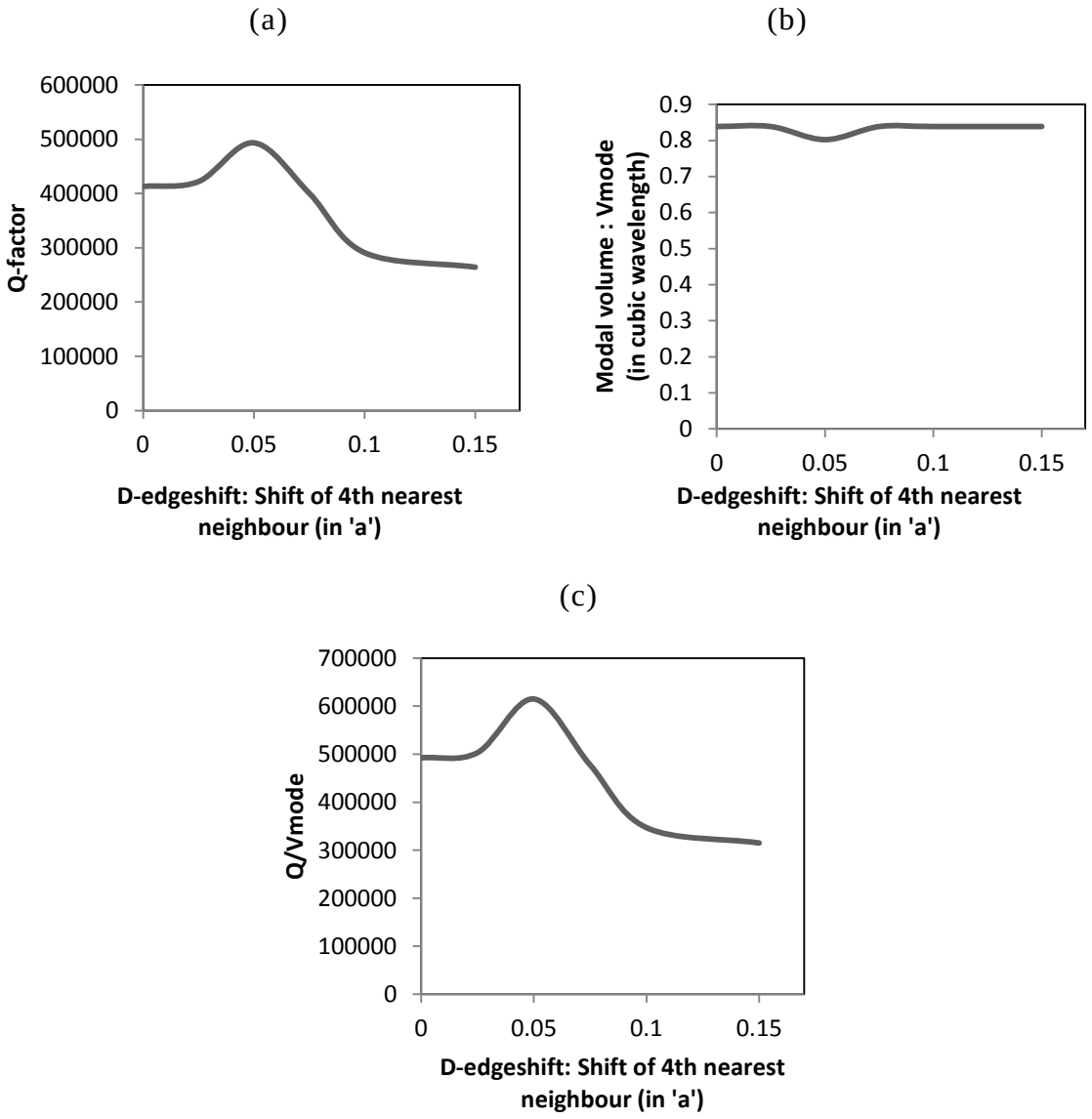


**Fig. 4.11:** Variation of (a) Q-factor, (b) $V_{mode}$ and (c) $Q/V_{mode}$ with 'D' air-hole displacements (maximum Q-factor obtained for D-edgeshift of 0.05 with not much variation in modal volume)

The ultra-high value of Q-factor indicates strong light confinement. Small value of mode volume indicates that light is localized in the cavity. Thus, the light is both temporally and spatially confined. A large $Q/V_{mode}$ indicates a large Purcell factor. Hence, a strong light-matter interaction can be achieved.

### 4.4.4 Calculation of Resonant wavelength and Spectral Width

**i) Resonant wavelength**

From FDTD simulations of cavity structure, we have obtained a resonant frequency of 0.258 c/a. Considering lattice constant a=235 nm,

Resonant frequency,

$$f_{resonant} = 0.258 \times \frac{(3 \times 10^8)}{(235 \times 10^{-9})} = 329.44 \text{ THz}$$

Resonant wavelength [1],

$$\lambda_{resonant} = \frac{c}{f_{resonant}} \quad (4.1)$$

$$= \frac{3 \times 10^8}{329.44 \times 10^{14}} = 910.625 \text{ nm}$$

Cavity length,

$$L_C = 3.8a = 3.8 \times (235 \times 10^9) = 893 \text{ nm}$$

This shows that resonant wavelength is comparable to cavity length

$$\text{i.e., } \lambda_{resonant} \sim L_C$$

Since, the cavity length is in nanometer range, it is a nanocavity.

**ii) Spectral width:**

Spectral width $\Delta\lambda$ is obtained from expression [1]

$$Q = \frac{\lambda_{resonant}}{\Delta\lambda} \quad (4.2)$$

For Q=493681 and $\lambda$=910.625 nm,

$$\Delta\lambda = \frac{493681}{910.625 \times 10^{-9}} = 1.84 \text{ pm}$$

Thus, we have obtained a single mode from L3 nanocavity with resonant wavelength of 910.625 nm and spectral width of 1.84 pm.

### 4.4.5 Calculation of Photon lifetime

The photon lifetime of the cavity mode is also computed to get an idea about the light confinement. It is given by the below formula [1]:

$$\tau_{ph} = \frac{Q}{2\pi f_{resonant}} \quad (4.3)$$

where, $\tau_{ph}$ denotes photon lifetime, Q and $f_{resonant}$ are the quality factor and resonant frequency of cavity mode respectively.

For Q= 493681 and $f_{resonant}$= 0.258 c/a ,

$$\tau_{ph} = \frac{493681}{2\pi * 0.258\ c/a}$$

$$\tau_{ph} = 304502.26\ a/c$$

For lattice constant a=235 nm, $\tau_{ph} =$ 238.47 ps or, 0.238 ns.

This lie in the range of anticipated spontaneous emission lifetime, which is 0.1 – 5 ns.

### 4.4.6 Effect of increasing slab thickness

By slightly increasing the slab-thickness to 0.65a from 0.6a discussed above and performing FDTD simulations for the photonic crystal cavity structure, a further increase in Q-factor to 577010 and $Q/V_{mode}$ to 695789$(\lambda/n)^{-3}$ is observed for single mode at resonant frequency 0.249 c/a, while the mode volume for this structure doesn't increase much and is 0.829$(\lambda/n)^3$, i.e., still less than a cubic wavelength. **Table 4.2** shows the variation of these parameters with slab thickness.

**Table 4.2:** Effect of increasing slab thickness

| **Slab thickness** in a | **Resonant frequency** in c/a | **Q-factor** | $\mathbf{V_{mode}}$ in $(\lambda/n)^3$ | $Q/\mathbf{V_{mode}}$ in $(\lambda/n)^{-3}$ |
|---|---|---|---|---|
| 0.6 | 0.258 | 493681 | 0.802 | 615152 |
| 0.65 | 0.249 | 577010 | 0.829 | 695789 |

## 4.5 Comparison with L3 cavity having six air-hole shifts

For L3 cavity as reported in reference 28, Q-factor increases by a factor of 44 and $Q/V_{mode}$ increases by factor of 40 in comparison to unoptimised L3 Cavity on giving air-hole displacements to three nearest neighbour air-holes on cavity edges. However, in our cavity by shrinking the first nearest neighbour air holes and shifting fourth nearest neighbour air holes in addition to three nearest neighbour

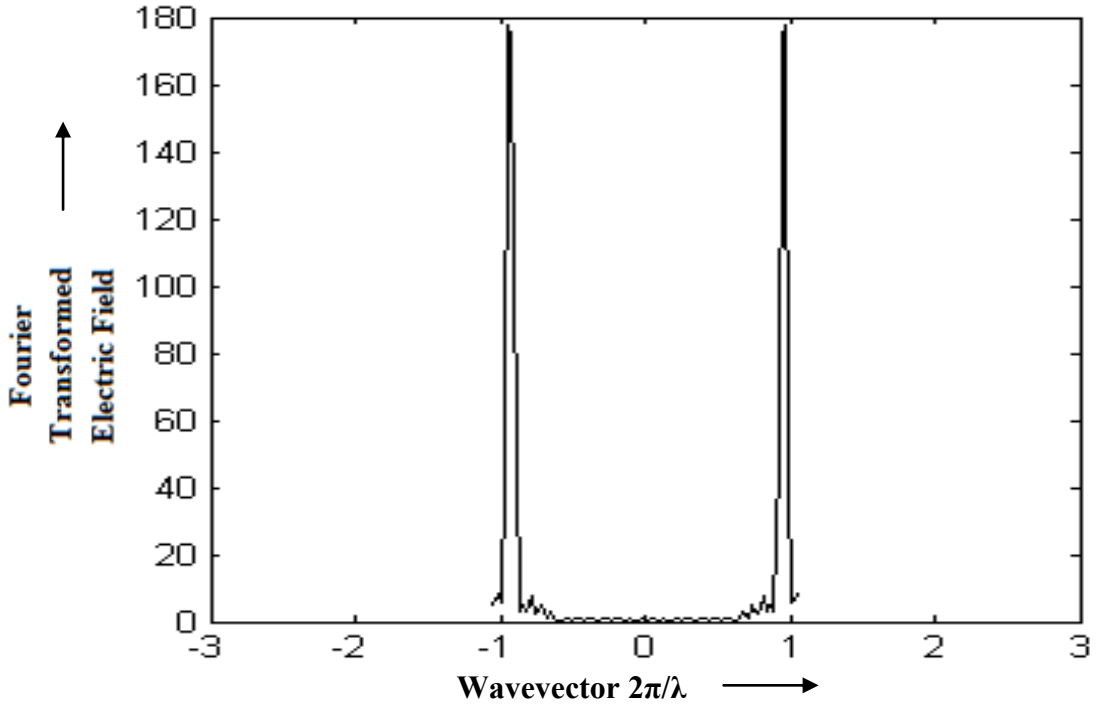


(a)

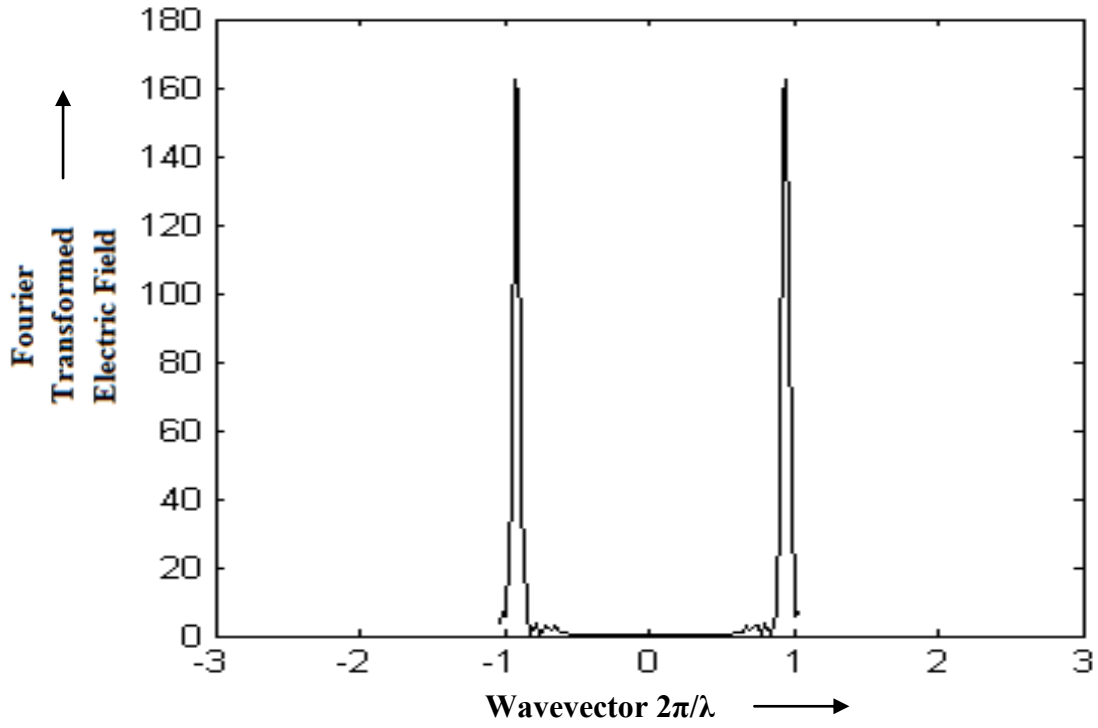


(b)

**Fig. 4.12:** Comparison of spatial fourier transformed electric field for (a) optimised cavity with three nearest neighbour air hole displacements and (b) optimized cavity with four nearest neighbour air-hole displacements and 1$^{st}$ nearest neighbour air-holes shrinkage

air-hole displacements, an improvement by a factor of 84 in Q-factor and by a factor of 70 in $Q/V_{mode}$ is obtained in comparison to unoptimized L3 Cavity.

This can be attributed to further reduction in energy losses or leaky modes that couple to continuum of radiation modes in light cone. It can be understood by studying the spatial fourier transform of electric field distribution of cavity modes. Reduction in wavevectors |k| in the range 0 to $2\pi/\lambda$ in the **Fig. 4.12(b)** in comparison to **Fig. 4.12(a)** indicates an increase in Q-factor and hence Q/Vmode.

# CHAPTER 5
# CONCLUSION & FUTURE SCOPE

In this thesis, we endeavour to further understand photonic crystal nanocavities, which confine and manipulate photons on the nanometer scales. We have taken an air-bridged photonic crystal structure made out of GaAs with triangular array of air-holes and have created a L3 cavity (with three missing air-holes in the center). In order to strengthen light-matter interaction in cavity, we investigated the parameters quality factor, mode volume and $Q/V_{mode}$ . We have proposed a cavity design which is based on gradual confinement of cavity's resonant mode and reduction of leaky wave-vector components in the light cone. We have reduced the in-plane losses by increasing the number of photonic crystal layers around the cavity, and reduced the out-of-plane losses by shifting the four nearest neighbour air-holes on cavity edges and shrinking first nearest neighbour air-holes on cavity edges. As a result, we have obtained a single cavity mode at resonant frequency 0.258 c/a with Q-factor 493681, mode volume $0.828(\lambda/n)^3$ and $Q/V_{mode}$ of $615152(\lambda/n)^{-3}$. This design improves the quality factor by a factor of 84 and $Q/V_{mode}$ by a factor of 70 in comparison to unoptimised L3 photonic crystal nanocavity. The mode volume for the given design is less than $(\lambda/n)^3$.

Such photonic crystal nanocavities lead to very large Purcell factor because of their ultra-high Q-factor and ultra-small cavity mode volume. They can be used for realization of quantum computing platform by coupling with quantum dots and nanocavity LASER.

The next recommended effort may focus on coupling a quantum dot in the high performance PhC nanocavity and building a strong interacting system. Such a system can be a possible platform for realising a practical, scalable quantum computer. Another area of future research can be the design of high performance photonic crystal nanocavity with efficient vertical emission for the realisation of nanocavity LASER.

# REFERENCES


[1] J. D. Joannopoulos, S. G. Johnson, J. N. Winn, R. D. Meade, "Photonic Crystals - Molding the flow of light", 2nd Edition, *Princeton University Press*, 2008.

[2] L. Weng, "An Introduction to Photonic Crystals", LC Optics and Photonics Course, *Kent State University*, 2012.

[3] E. Yablonovitch, "Inhibited spontaneous emission in solid-state physics and electronics", *Physical Review Letters*, Vol. 58, pp. 2059−2062, 1987.

[4] S. John, "Strong Localization of Photons in Certain Disordered Dielectric Superlattices", *Physical Review Letters*, Vol. 58, No.23, pp. 2486-2489, 1987.

[5] J.D. Joannopoulos, P. R. Villeneuve & S. Fan, "Photonic Crystals: putting a new twist on light", *Nature*, Vol. 386, No. 6621, pp. 143-149, 1997.

[6] A. Mock and L. Lu, "Two-Dimensional Photonic Crystal Microcavities for Chip-scale Laser Applications", *Recent Optical and Photonic Technologies*, ISBN 978-953-7619-71-8, pp. 450, 2010.

[7] Y. Akahane, T. Asano, B. S. Song, & S. Noda, "High-Q photonic nanocavity in a two-dimensional photonic crystal", *Nature*, Vol. 425, No. 6961, pp. 944-947, 2003.

[8] S. Prorok, "Nanophotonics and integrated optics: Photonic Crystal Cavities", *CST AG*, 2013.

[9] S. Noda, "Recent Progresses and Future Prospects of Two- and Three-Dimensional Photonic Crystals", *Journal of Lightwave Technology*, Vol. 24, No. 1, pp. 4554-4567, 2006.

[10] A. Daraeia and M. Daraei, "Confined Photonic Modes in the Photonic Crystals L3 Line Defect Nanocavities", *Proceedings of the 4th International Conference on Nanostructures* (ICNS4), Kish Island, I.R. Iran, 2012.

[11] T. W. Saucer, & V. Sih, "Optimizing nanophotonic cavity designs with the gravitational search algorithm" *Optics Express*, Vol. 21, No. 18, pp. 20831-20836, 2013.

[12] K. J. Vahala, "Optical microcavities", *Nature*, Vol. 424, No. 6950, pp. 839-846, 2003.

[13] L. Lalouat, B. Cluzel, C. Dumas, L. Salomon, and F. de Fornel. "Imaging photoexcited optical modes in photonic-crystal cavities with a near-field probe", *Physical Review B*, Vol. 83, No. 11, pp. 115326, 2011.

[14] M. Lončar, T. Yoshie, A. Scherer, P. Gogna, and Y. Qiu, "Low-threshold photonic crystal laser", *Applied Physics Letters*, Vol. 81, No. 15, pp. 2680-2682, 2002.

[15] H. Takagi, Y. Ota, N. Kumagai, S. Ishida, S. Iwamoto, and Y. Arakawa, "High Q H1 photonic crystal nanocavities with efficient vertical emission", *Optics Express*, Vol. 20, No. 27, pp. 28292-28300, 2012.

[16] J. Hagemeier, C. Bonato, T. A. Truong, H. Kim, G. J. Beirne, M. Bakker, M. P. van Exter, Y. Luo, P. Petroff, and D. Bouwmeester, "H1 photonic crystal cavities for hybrid quantum information protocols." *Optics Express*, Vol. 20, No. 22, pp. 24714-24726, 2012.

[17] T. Tanabe, A. Shinya, E. Kuramochi, S. Kondo, H. Taniyama, & M. Notomi, "Single point defect photonic crystal nanocavity with ultrahigh quality factor achieved by using hexapole mode", *Applied Physics Letters*, Vol. 91, No. 2, pp. 021110, 2007.

[18] E. Kuramochi, E. Grossman, K. Nozaki, K. Takeda, A. Shinya, H. Taniyama, and M. Notomi, "Large Q factor enhancement of Ln nanocavity by a unified hole-shifting rule", Conference on Lasers and Electro-Optics/ Pacific Rim, Optical Society of America, 2013.

[19] C. W. Wong, X. Yang, C. Chen, C. Husko, "Systems, devices and methods for tuning a resonant wavelength of an optical resonator and dispersion properties of a photonic crystal waveguide", US Patent 8705898 B2, July 16, 2008.

[20] J. Riedrich-Möller, L. Kipfstuhl, C. Hepp, E. Neu, C. Pauly, F. Mücklich, A. Baur, "One-and two-dimensional photonic crystal microcavities in single crystal diamond", *Nature Nanotechnology*, Vol. 7, No. 1, pp. 69-74, 2012.

[21] W. Fan, Z. Hao, E. Stock, J. Kang, Y. Luo, and D. Bimberg. "Comparison between two types of photonic-crystal cavities for single-photon

emitters", *Semiconductor Science and Technology*, Vol. 26, No. 1, pp. 014014, 2011.

[22] B. S. Song, S. Noda, T. Asano, Y. Akahane, "Ultra-high-Q photonic double heterostructure nanocavity", *Nature Publishing Group*, Vol. 4, No. 3, 2005.

[23] H. Altug, Physics and Applications of Photonic Crystal Nanocavities, Dissertation, *Stanford University*, 2006.

[24] N.A. Saulnier, "Computational Modelling of Photonic Crystal Microcavity Single-Photon Emitters", Dissertation, *Carnegie Mellon University*, 2011.

[25] T. Yoshie, J. Vuckovic, A. Scherer, H. Chen, and D. Deppe, "High quality two-dimensional photonic crystal slab cavities", *Applied Physics Letters*, Vol. 79, pp. 4289–4291, 2001.

[26] S. Noda, M. Imada, M. Okano, S. Ogawa, M. Mochizuki, & A. Chutinan, "Semiconductor three-dimensional and two-dimensional photonic crystals and devices", *IEEE Journal of Quantum Electronics*, Vol. 38, No. 7, pp. 726-735, 2002.

[27] C. Xiang-Hua, Z. Wan-Hua, M. Xiao-Tao, R. Gang, and X. Jian-Bai, "Two-dimensional photonic band-gap defect modes with deformed lattice", *Chinese Physics Letters*, Vol. 22, No. 9, pp. 2290, 2005.

[28] Y. Akahane , T. Asano , B. S. Song , & S. Noda, "Fine-tuned high-Q photonic-crystal nanocavity", *Optics Express*, Vol. 13, No. 4, pp. 1202-1214, 2005.

[29] D. Englund and I. Fushman, "General recipe for designing photonic crystal cavities", Optical Society of America, *Optics Express*, Vol. 12, No. 16, pp. 5961-5975, 2005.

[30] L. Chen and E. Towe, "Design of High-Q Microcavities for proposed 2-D Electrically pumped Photonic Crystal Lasers", *IEEE Journal In Quantum Electronics*, Vol. 12, No. 1, pp. 117-123, 2006.

[31] A. Tandaechanurat, S. Iwamoto, M. Nomura, N. Kumagai, and Y. Arakawa, "Increase of Q-factor in photonic crystal H1-defect nanocavities after closing of photonic bandgap with optimal slab thickness", *Optics Express*, Vol. 16, No. 1, pp. 448-455, 2008.

[32] M. Fujita, Y. Tanaka and S. Noda, "Light Emission from Silicon in Photonic Crystal Nanocavity", *IEEE Journal of Quantum Electronics*, Vol. 14, No. 4, pp. 1090-1097, 2008.

[33] M. Notomi, E. Kuramochi, and H. Taniyama. "Ultrahigh-Q nanocavity with 1D photonic gap", *Optics Express,* Vol. 16, No. 15, pp. 11095-11102, 2008.

[34] P. B. Deotare, M. W. McCutcheon, I. W. Frank, M. Khan, and M. Lončar, "High quality factor photonic crystal nanobeam cavities", *Applied Physics Letters*, Vol. 94, No. 12, pp. 121106, 2009.

[35] J. Sweet, B. C. Richards, J. D. Olitzky, J. Hendrickson, G. Khitrova, H. M. Gibbs, D. Litvinov, "GaAs photonic crystal slab nanocavities: Growth, fabrication, and quality factor", *Photonics and Nanostructures-Fundamentals and Applications,* Vol. 8, No. 1, pp. 1-6, 2010.

[36] J. R. Pugh, Y. D. Ho, E. Engin, C. Railton, J. G. Rarity, and M. J. Cryan, "Novel high-Q modes in thick 2D photonic crystal slabs", *Journal of Optics*, Vol. 15, No. 3, pp. 035004, 2013.

[37] I. J. Luxmoore, R. Toro, O. Del Pozo-Zamudio, N. A. Wasley, E. A. Chekhovich, A. M. Sanchez, R. Beanland, A. M. Fox, M. S. Skolnick, H. Y. Liu & A. I. Tartakovskii, "III-V quantum light source and cavity-QED on Silicon", *Scientific reports* 3, No. 1239, 2013.

[38] P.T. Lee, T.W. Lu and L.H. Chiu, "Dielectric-Band Photonic Crystal Nanobeam Lasers", *IEEE Journal Of Lightwave Technology*, Vol. 31, No. 1, pp. 36-42, 2013.

[39] A. F. Oskooi, D. Roundy, M. Ibanescu, P. Bermel, J. D. Joannopoulos, and Steven G. Johnson, "MEEP: A flexible free-software package for electromagnetic simulations by the FDTD method", *Computer Physics Communications*, Vol. 181, No. 3, pp. 687-702, 2010.

[40] http://ab-initio.mit.edu/wiki/index.php/MEEP

[41] W. R. Frei, H. T. Johnson, and Kent D. Choquette, "Optimization of a single defect photonic crystal laser cavity", *Journal of Applied Physics*, Vol. 103, No. 3, pp. 033102, 2008.

[42] T. Asano, B. S. Song, Y. Akahane, and S. Noda, "Ultra high-Q nanocavities in two-dimensional photonic crystal slabs," *IEEE Journal of Selected Topics in Quantum Electronics*, Vol. 12, pp. 1123, 2006.

[43] J. Vučković, M. Lončar, H. Mabuchi, and A. Scherer. "Design of photonic crystal microcavities for cavity QED", *Physical Review E,* Vol. 65, No. 1, pp. 016608, 2001.

[44] L. C. Andreani, D. Gerace, and M. Agio, "Exciton-polaritons and nanoscale cavities in photonic crystal slabs", *Physica Status Solidi* (b), Vol. 242, No. 11, pp. 2197–2209, 2005.

[45] F. Shanhui, M. F. Yanik, Z. Wang, S. Sandhu, and M. L. Povinelli, "Advances in Theory of Photonic Crystals", *Journal of Lightwave Technology*, Vol. 24, No. 12, pp. 4493-4501, 2006.

[46] P. Bhattacharya, J. Sabarinathan, W. D. Zhou, P.C. Yu, A. McGurn, "Electrically Injected Photonic Crystal Microcavity Light Sources May Realize High-Efficiency Single-Mode LEDs", *IEEE Circuits & Devices Magazine*, Vol. 19, No. 2, pp. 25-33, 2003.

[47] D. W. Prather, S. Shi, J. Murakowski, G. J. Schneider, A. Sharkawy, C. Chen, & B. Miao, "Photonic Crystal Structures and Applications: Perspective, Overview, and Development", *IEEE Journal of Quantum Electronics*, Vol. 12, No. 6, pp. 1416-1437, 2006.

[48] P.V. Braun, S. A. Rinne, and F. García-Santamaría, "Introducing Defects in 3D Photonic Crystals: State of the Art", *Advanced Materials*, Vol. 18, No. 20, pp. 2665-2678, 2006.

[49] X Serey, S. Mandal, and D. Erickson, "Comparison of Silicon Photonic Crystal Resonator designs for optical trapping of Nanomaterials", *Nanotechnology*, Vol. 21, No. 30, pp. 305202, 2010.

[50] M.A. Miri, A. Khavasi, M. Miri, and K. Mehrany, "A Transmission Line Resonator Model for Fast Extraction of Electromagnetic Properties of Cavities in Two-Dimensional Photonic Crystals", *IEEE Journal of Photonics*, Vol. 2, No. 4, pp. 677-685, 2010.

[51] E. P. Karabulut and M. Irsadi Aksun, "Characterization of Finite Photonic Crystals with Defects", *IEEE Journal of Quantum Electronics*, Vol. 47, No. 3, pp. 406-413, 2011.

[52] X. Chew, G. Zhou, F. S. Chau, and J. Deng, "Nanomechanically Tunable Photonic Crystal Resonators Utilizing Triple-Beam Coupled Nanocavities", *IEEE Photonics Technology Letters*, Vol. 23, No. 18, pp. 1310-1312, 2011.

[53] G. Shambat, B. Ellis, J. Petykiewicz, M. A. Mayer, A. Majumdar, T. Sarmiento, J. S. Harris, E. E. Haller, and J. Vuckovic, "Electrically Driven Photonic Crystal Nanocavity Devices", *IEEE Journal of Quantum Electronics*, Vol. 18, No. 6, pp. 1700-1710, 2012.

[54] J. O. Kjellman, T. Tanemura, and Y. Nakano, "Optimization of Compact Photonic Crystal Cavity Using the Gentle Confinement Method", Photonics Society Summer Topical Meeting Series, *IEEE*, pp. 44-45, 2013.

[55] D. Wang, Z. Yu, Y. Liu, X. Guo, C. Shu, S. Zhou, and J. Zhang, "Ultra-small modal volume and high Q factor optimization of a photonic crystal slab cavity", *Journal of Optics,* Vol. 15, No. 12, pp. 125102, 2013.

[56] H. Takano, Y. Akahane, T. Asano, and S. Noda, "In-plane-type channel drop filter in a two-dimensional photonic crystal slab", *Applied Physics Letters,* Vol. 84, pp. 2226-2228, 2004.

[57] H. Sekoguchi, Y. Takahashi, T. Asano, and S. Noda, "Photonic crystal nanocavity with a Q-factor of~ 9 million", *Optics Express,* Vol. 22, No. 1, pp. 916-924, 2014.

[58] R. Bose, D. Sridharan, H. Kim, G. S. Solomon, and E. Waks, "Low-photon-number optical switching with a single quantum dot coupled to a photonic crystal cavity", *Physical Review Letters,* Vol. 108, No. 22, pp. 227402, 2012.

[59] S.H. Kwon, T. Sünner, M. Kamp, and A. Forchel, "Optimization of photonic crystal cavity for chemical sensing", *Optics Express,* Vol. 16, No. 16, pp. 11709-11717, 2008.